Chemical Geology 522 (2019) 38–54

Contents lists available at ScienceDirect

Chemical Geology

journal homepage: www.elsevier.com/locate/chemgeo

Controls on the geochemistry of suspended sediments from large tropical South American rivers (Amazon, Orinoco and Maroni)

Tristan C.C. Rousseau[a,b,*], Martin Roddaz[a], Jean-Sébastien Moquet[c], Helga Handt Delgado[d], Gérôme Calves[a], Germain Bayon[e]

[a] GET, Université de Toulouse, CNRS-IRD-OMP, 14 avenue Edouard Belin, 31400 Toulouse, France
[b] LABOMAR-Universidade Federal do Ceará, Av. da Abolição, 3207, Fortaleza 60165-081, CE, Brazil
[c] Institut de Physique du Globe de Paris -, Centre National de la Recherche Scientifique, 1 rue Jussieu, 75005 Paris, France
[d] Instituto Venezolano de Investigaciones Cientificas, IVIC Centro de Oceanologia y Estudios Antárticos Carretera Panamericana, Km 11. Altos de Pipe 1020ª Venezuela
[e] IFREMER, Unité de Recherche Géosciences Marines, F-29280 Plouzané, France

ARTICLE INFO

Editor: Michael E. Böttcher

Keywords:
Major and trace elements
Nd–Sr isotopes
Suspended sediments
Yearly hydrological cycle
Amazon River
Orinoco River
Maroni River

ABSTRACT

We report mineralogical, elemental (major and trace elements) and Sr–Nd isotopic data for suspended particulate matter (SPM) samples from the Amazon, Orinoco and Maroni Rivers collected on a monthly basis over a one-year long hydrological cycle. The aim of this study was i) to characterize the mineralogical and geochemical composition of major South American tropical rivers and ii) to evaluate the effect of seasonal hydroclimate variations and changes in sediment discharge on the composition of these SPM. In addition to displaying particular mineralogical and geochemical signatures (e.g. Al/Si ratios, weathering indices), the Amazon, Orinoco and Maroni SPM are characterized by marked differences in $^{87}Sr/^{86}Sr$ (0.7213 ± 0.0030, 0.7288 ± 0.0018 and 0.7335 ± 0.0019, respectively), and εNd values (−10.6 ± 0.6, −14.1 ± 0.3 and −23.7 ± 1.2), which reflect differences in source rock lithology. While we find no effect of the hydrological cycle on the geochemistry of Orinoco SPM, particulate εNd and Cr/Th signatures fluctuate with the hydrological cycle in the Maroni basin, indicating that they are controlled by variation in rainfall distribution linked to the latitudinal migration of the Intertropical Convergence Zone (ITCZ). In contrast to Maroni and Orinoco SPM, the Amazon SPM are characterized by significant Sr isotope annual variability correlated with suspended sediments discharge and a small but significant Nd isotopic variability over the year. This latter variation is related to seasonal changes in the rainfall distribution patterns across the Amazon basin, associated with latitudinal migrations of the ITCZ. This suggests that the geochemical composition of the SPM exported over the year from the Amazon Basin faithfully responds to hydroclimate changes related associated with the migration of the rain belt over regions of contrasted geochemical signatures.

These findings have implications for the application of Sr and Nd isotopes as provenance proxies in sedimentary archives and paleoclimatic studies. The Sr isotopic composition of exported SPM appears to be mostly controlled by weathering processes and/or mineralogical sorting, rather than being indicative of sediment provenance. In contrast, the relationship documented between Nd isotopes and the hydrological variability indicates that their application to archives of past river sediment discharges can provide unique insights on paleo-hydroclimate changes over tropical South America.

1. Introduction

Rivers are the main providers of freshwater and sediment issued from the continents to the oceans. Characterizing land-sea sediment transfers from large river systems is essential for reconstructing global geochemical cycles and nutrient inputs into the oceans, as well as for estimating the fluxes of atmospheric CO_2 consumed by silicate weathering and organic carbon burial (Gaillardet et al., 1999; Galy et al., 2007; Meybeck, 1993).

Tropical regions display the world highest rainfall rates and are also particularly sensitive to climate variability (Syvitski et al., 2014; Syvitski and Milliman, 2007), hence with large impact on sediment production and global biogeochemical cycles (Hamilton, 2010; Milliman and Farnsworth, 2011a; Milliman and Farnsworth, 2011b;

* Corresponding author at: GET, Université de Toulouse, CNRS-IRD-OMP, 14 avenue Edouard Belin, 31400 Toulouse, France.
E-mail address: tristanrousseau@ufc.br (T.C.C. Rousseau).

https://doi.org/10.1016/j.chemgeo.2019.05.027
Received 28 May 2018; Received in revised form 15 May 2019; Accepted 17 May 2019
Available online 21 May 2019

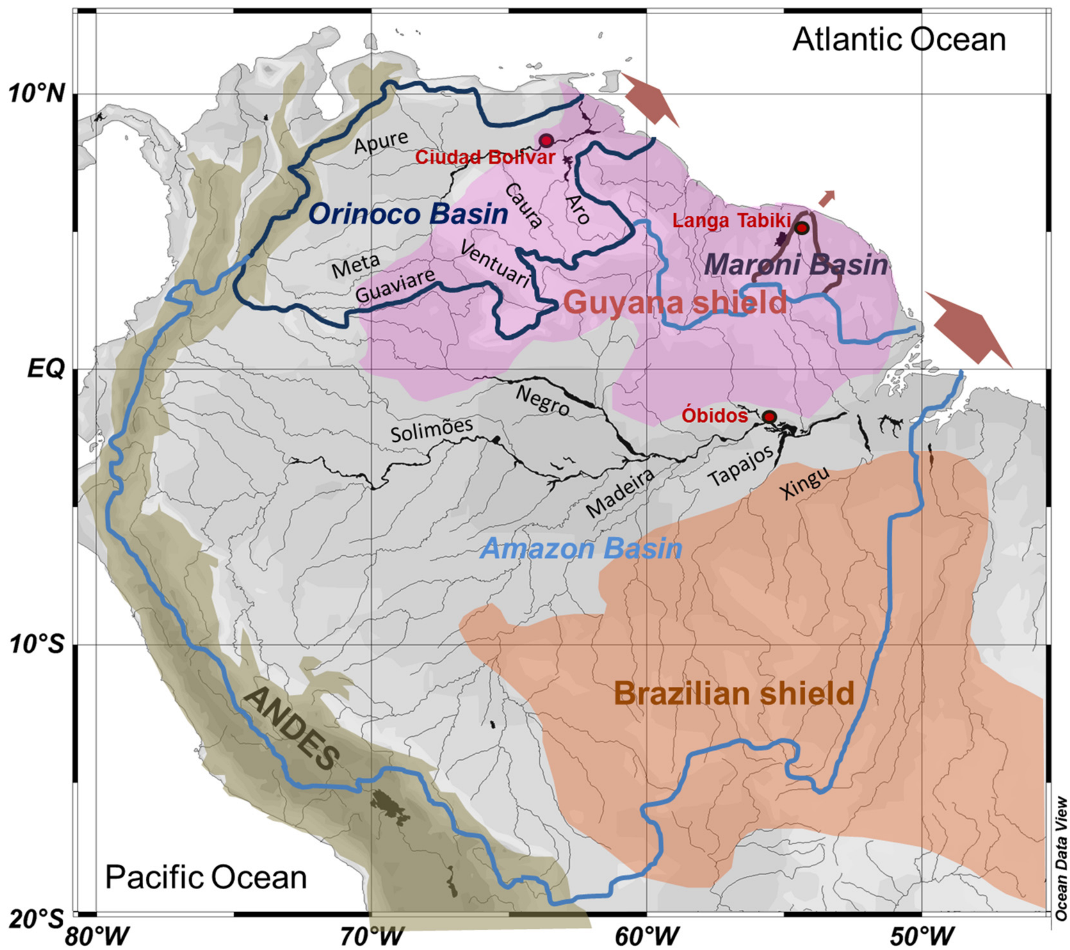

Fig. 1. Map representing the drainage basin of the Amazon (light blue), Orinoco (dark blue) and Maroni Rivers (brown) together with the Andes, the Guyana and Brazilian shields. The red dots indicate the location of the hydrological station where suspended particulate matter (SPM) were sampled (i.e. Ciudad Bolivar for the Orinoco, Langa Tabiki for the Maroni and Óbidos for the Amazon). The width of the arrows represent the sediments fluxes of the rivers. (For interpretation of the references to colour in this figure legend, the reader is referred to the web version of this article.)

Syvitski et al., 2003). Previous studies have suggested that the geochemical composition of suspended particulate matter (SPM) and other fine-grained sediments preserved in sedimentary records could reflect past hydrological fluctuations in river basins (e.g. Chiessi et al., 2009; Govin et al., 2014). However, the utility of SPM-based geochemical proxies for paleoclimate studies is complicated by the fact that in tropical/equatorial regions, the chemical and mineralogical composition of the sediment transported by rivers is also strongly dependent on the degree of chemical weathering, the lithology of corresponding drainage basins, and various grain-size effects (Bouchez et al., 2011).

The Amazon and the Orinoco Rivers are the main South American rivers in terms of dissolved and solid fluxes exported to the oceans (Fig. 1). The SPM transported by the Amazon River has already been the subject of a number of studies that provided estimates for sediment fluxes and present-day physical denudation rates (Filizola and Guyot, 2004; Gaillardet et al., 1997; Milliman and Meade, 1983). The chemical and mineralogical characterization of Amazon River sediments has also been used i) for provenance studies (Basu et al., 1990; Guyot et al., 2007; Guyot et al., 1999; Martinelli et al., 1993; Roddaz et al., 2005; Roddaz et al., 2006; Vital and Stattegger, 2000; Wittmann et al., 2011); ii) to investigate weathering patterns in the Andean mountains and the lowland regions (Allègre et al., 1996; Gaillardet et al., 1997; Gibbs, 1967; Guyot et al., 2007; Sawakuchi et al., 2018; Viers et al., 2008); iii) to constrain sediment residence time within the Amazon Basin (Aalto et al., 2006; Dosseto et al., 2006; Dunne et al., 1998; Meade et al., 1985; Wittmann et al., 2011); and iv) to estimate the chemical composition of the upper continental crust and its evolution through geological time (Allègre et al., 1996; Gaillardet et al., 1997; Goldstein and Jacobsen, 1988; Goldstein et al., 1984). Recent studies have shown that sediment concentration and grain-size distribution of the suspended sediment load in the Amazon Basin was mainly controlled by hydrodynamic sorting (Bouchez et al., 2011). Grain-size sorting can lead to chemical stratification of the SPM in the Amazon River, with suspended sediment loads from the Madeira and Solimões Rivers (i.e. the two main Andean tributaries of the Amazon; Fig. 1) being preferentially transported in surface waters and at depth, respectively (Bouchez et al., 2011). In addition, the Sr isotopic composition of Madeira and Solimões SPM varies in phase with SPM concentrations throughout the hydrological cycle (Viers et al., 2008). This relationship has been ascribed to the fact that increasing physical weathering during the rainy season favours landslides and river bank erosion, which in turn lead to the export of sediments that are generally mobilized under high runoff conditions. To date however, it remains unclear whether or not a similar control of the hydrological cycle on the geochemistry of SPM also exists further downstream of the Amazon Basin, near the mouth of the river.

In comparison with the Amazon River, the Orinoco SPM has received far less attention. No study has ever dealt with the processes that control the geochemistry of the Orinoco SPM. It is unclear whether the hydrological control demonstrated for the SPM composition of the Solimões and Madeira Rivers (Viers et al., 2008) also applies to other large rivers in tropical/equatorial South America. Assessing whether such hydrological control exists on the Sr–Nd isotopic compositions of

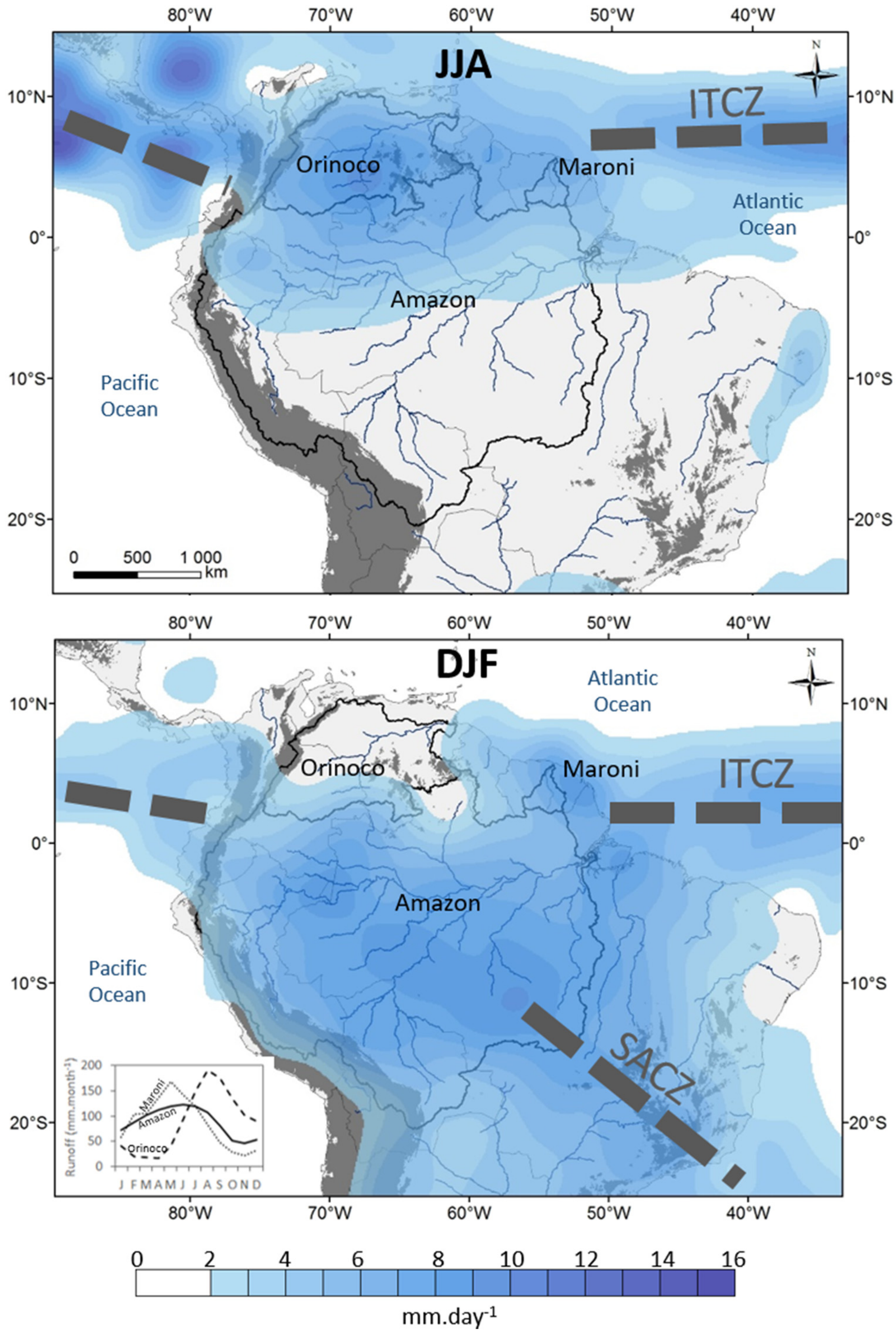

Fig. 2. 1986–2015 average rainfall distribution over northern South America during JJA (June–July-August) and DJF (December–January-February) periods (source: CAMSOPI data through clim explorer website https://climexp.knmi.nl). The 1986–2015 monthly runoff average for Amazon, Orinoco and Maroni Rivers basins is added for reference.

SPM is important because Nd isotopes, and to a lesser extent Sr, are being increasingly used in marine sediment records from the Atlantic Ocean to investigate paleoclimatic variations in South America over various geological timescales (e.g. Hoorn et al., 2017; Höppner et al., 2018; van Soelen et al., 2017; Zhang et al., 2015). The SPM exported by the Solimões and Madeira Rivers is mainly derived from erosion of the Andes. However, smaller rivers like the Maroni (French Guiana) drain exclusively older shield areas, and therefore most likely transport SPM having very contrasted geochemical compositions by comparison with active mountainous SPM sources.

In this study, we report on a detailed investigation of Sr—Nd isotopic compositions as well as major and trace element concentrations of SPM from the Amazon, Orinoco and Maroni Rivers, sampled on a monthly-basis over a year-long hydrological cycle. The main goals of this study were i) to characterize the isotopic and geochemical composition of SPM in these rivers, and ii) to evaluate possible systematic temporal variations in the Sr—Nd isotope and geochemical compositions of the SPM during the hydrological cycle.

2. Study area

Together, the Amazon (5.96×10^6 km^2), Orinoco (1.04×10^6 km^2) and Maroni (0.06×10^6 km^2) river basins occupy around 42% of the entire South American continent, ranging from about 10°N to 20°S and from 50°W to 80°W (Fig. 1). The Amazon River ranks first in terms of global mass transfer from the continents to the oceans, supplying about 17% of the freshwater (Callède et al., 2010), ~7% of the dissolved load (Moquet et al., 2016) and ~3% of the suspended load (Filizola et al., 2011; Guyot et al., 2005; Martinez et al., 2009; Milliman and Farnsworth, 2011b) discharged to the world's oceans. The Orinoco River is the third world river in terms of water discharge (Dai and Trenberth, 2002; Laraque et al., 2013b) and contributes to 3%, 0.8% and 0.5% of the water, dissolved inputs and suspended loads annually exported by world rivers to the oceans, respectively (Laraque et al., 2013a).

Three main geological domains are drained by these rivers: the Andes mountain range, sedimentary plains and shield areas. The Andes covers 15% and 12% of the Orinoco and Amazon River basins, respectively. In both basins, the Andes display a large diversity of lithologies that include evaporites, carbonates, granitic rocks, Palaeozoic sedimentary rocks and andesite volcanic rocks (Ahlfeld and Branisa, 1960; Baldock, 1982; INGEMMET, 1999; SERGEOMIN and YPFB, 2000). Sedimentary plains are generally fed by sediments from the Andean mountain range (Junk and Sioli, 1984; Roddaz et al., 2014). In this area, floodplain lakes (*várzeas*) along the main channels of the Orinoco and Amazon Rivers are seasonally flooded (Dunne et al., 1998; Martinez and Le Toan, 2007; Mertes et al., 1996), playing a significant role in the export of SPM to the main river channel (Bonnet et al., 2008; Bourgoin et al., 2007; Viers et al., 2005). South American shields consist of Precambrian terranes, which provide limited sediment contribution to total solid fluxes carried by both the Amazon and Orinoco basins (Furch and Junk, 1982; Konhauser et al., 1994).

The Solimões and Madeira Rivers are the two main tributaries of the Amazon River issued from the Andean mountains (Fig. 1). Together, these two rivers account for approximately 64% of the total water discharge (Moquet et al., 2016) and almost the entire sediment load annually delivered by the Amazon (Armijos et al., 2013a; Armijos et al., 2013b; Filizola et al., 2011; Laraque et al., 2013a; Laraque et al., 2013b; Moquet et al., 2016). The Negro River drains the Guyana shield in the northern portion of the Amazon, representing 17% of the Amazon water discharge (Moquet et al., 2016). The Tapajos and the Xingu represent together 10% of the Amazon water discharge and drain the Brazilian shield. Despite a significant contribution in water discharge, the Negro, Tapajos and Xingú Rivers carry very little amount of SPM and account for only 1–2% of the Amazon sedimentary flux export (Filizola et al., 2011; Filizola and Guyot, 2009).

The Orinoco River receives on its left-bank (northern) margin the Guaviare, Meta, Arauca and Apure Rivers, which drain the northern part of the Andean oriental cordillera and the *llanos* alluvial deposit. Together, they account for approximately 46% and 90% of the total water and sediment discharge, respectively (Meade, 1994). On its right-bank (southern) margin, the Ventuari, Caura and Caroni River tributaries drain the Guyana shield, and account for a total of 54% of the water discharge, but they contribute to a negligible part of the sediment load (Meade, 1994). By contrast, the Maroni River drains exclusively the Paleoproterozoic terranes of the Guyana shield and exhibit a low content in SPM and dissolved load (Sondag et al., 2010).

The hydroclimate patterns of the studied river basins and associated hydrological regimes are mainly controlled by the Southern American monsoon system (SAMS; Zhou and Lau, 1998) and is dependent on the seasonal variation of the continent–ocean temperature gradients and the migration of the Intertropical Convergence Zone (ITCZ), which moves southward (northward) during the austral summer (winter) (Fig. 2; Marengo, 2004; Marengo et al., 2012; Raia and Cavalcanti, 2008). As a consequence, a north–south gradient is typically observed in rainfall rates and seasonality (Espinoza Villar et al., 2009; Molina-Carpio et al., 2017). The Orinoco Basin and the northern and north-–western regions of Amazonia receive high rainfall associated with a low seasonality, whereas south-western and southern Amazonia experience lower rainfall associated with high seasonality (i.e. dry and wet seasons during austral winter and summer, respectively). As a consequence, the high discharge periods of the Orinoco, Maroni and Amazon Rivers successively occur from July to October, June to July and March to August, respectively (Guimberteau et al., 2012). The Amazon River exhibits a longer high discharge period because of the phase shift of its main tributaries maximum discharge (Bouchez et al., 2017; Moquet et al., 2016). These three basins exhibit a similar range of annual runoff with values ranging between 835 and 1090 mm/yr. However, the seasonality Index (SI), which is the ratio between the highest monthly discharge divided by the lowest one, is much higher for Maroni and Orinoco Rivers, with an SI of around 11, than for Amazon River which exhibits an SI of around 3.

3. Materials and methods

3.1. Sampling

Suspended particulate samples from the Amazon, the Orinoco and the Maroni Rivers were collected by the HYBAM observatory (http://www.ore-hybam.org/) (Fig. 1). Because of its position upstream the confluence of the Amazon with the Tapajós and Xingu Rivers, the sampling station of Óbidos do not integrate the inputs of these rivers. However, these tributaries are negligible in term of sediment inputs. Mid-section surface river samples were collected monthly from February 2012 to January 2013 in the Amazon River at the Óbidos station (01.9225°S; 55.6753°W), from January to December 2008 in the Orinoco River at Ciudad Bolivar station (08.1536° N; 063.5361°W) and in the Maroni River at Langa Tabiki station (05.1401° S; 054.3551° W) (Fig. 1).

Daily river discharges are extracted from the HYBAM database (http://www.ore-hybam.org/). SPM concentrations were measured by sampling 300 ml of water, filtering and weighting SPM each month. All geochemical and mineralogical results presented in this study were conducted on these filters.

3.2. Analytical methods

3.2.1. Sample treatments

Sampling and filtration were done using pre-cleaned HDPE bottles and 0.22 µm polyethylsulfone (PES) Millipore® membranes, respectively. After drying and weighting, 1 cm^2 fractions of the filters were cut using Teflon scissors for X-ray diffraction analyses (XRD). Suspended particles were extracted from the remaining part of the filters by 3 to 5 repeated ultrasonic baths in ultra-pure water. Solutions were subsequently evaporated at 60 °C and samples were split into two aliquots having 5–10 mg of sediments each: one for major and trace element analyses and the other one for Nd and Sr isotopic analyses. The aliquots used for elemental analyses were mixed with 20 to 40 mg of LiB, mineralized by alkali fusion in a Fluxer® and subsequently dissolved and diluted in 2% v/v HNO_3. The aliquots for isotopic measurements were first treated with H_2O_2 for 24 h at ambient temperature, then digested in HNO_3 + HF for 36 h at 80 °C, and in HCl + HNO_3 for 36 h at 100 °C. Sr and Nd were separated by ion-exchange chromatography using Sr–SPEC, TRU–SPEC and LN–SPEC resins (Eichrom®). Ultrapure and double–distilled reagents were used for all digestion and separation steps.

3.2.2. Sample analyses

All analyses were performed at the Géosciences-Environnement-Toulouse (GET) Laboratory - Observatoire Midi-Pyrénées (OMP). XRD analyses were carried out using a G3000 Inel diffractometer (40 kV, 30 mA) and Ni-filtered CuKα1,2 radiation (λ = 1.5406 Å). Due to limited amounts of material, we did not perform the glycol treatment, which enables the distinction of inflating clays and allows determination of smectite and chlorite abundances. After subtracting blank filter spectra, peaks of quartz, mica + illite and kaolinite were integrated and converted to relative frequencies.

Major element analyses were done by ICP-OES (Horiba Jobin Yvon Ultima2). Trace element analyses were performed by Quadrupole ICPMS (AGILENT 7500 CE), using a four-point calibration and In/Re as internal standards to correct for instrumental drift and matrix effects. Rare earth elements (REE) abundances were corrected from oxide and hydroxide isobaric interferences following Aries et al. (2000). Measurement accuracy was assessed by processing 5 to 10 mg of the GA basalt reference material (CRPG; Centre de Recherches Pétrographiques et Géochimiques), with results being in good agreement with recommended values (Abbey, 1980). Blank values accounted for < 2% of the average sample signal, with the exception of Na analysed with ICP-OES (6%) and Cr, Co and Ni analysed with ICPMS (6%, 4% and 26% respectively). Despite overall satisfying accuracies on the concentrations determined for the GA reference material, we observed an important fluctuation in the absolute concentrations from one sample to another with 82% of RSD for the 12 Al_2O_3 measurements in the Amazon River SPM. This variation is unlikely to be affected by the variation in SPM concentrations and is higher than previous observations of 12% of RSD for the 18 Al_2O_3 measurements in the Amazon River SPM by Bouchez et al. (2011). Such dispersion in absolute concentrations is probably due to incomplete sample recovery after the 60 °C evaporation step. This bias did not affect the geological standard because standards were directly weighted without filter extraction. As a consequence, absolute concentrations given in this study should be cautiously used here and be considered as semi-quantitative only. However, this issue should not affect any interpretation based on inter-element relative concentrations (elemental ratios) in each sample, which hence can be used for discussion below.

Nd and Sr isotope measurements were conducted on a Thermo Finnigan MAT 261. Nd isotope ratios were measured in static mode, corrected for instrumental mass bias using a $^{146}Nd/^{144}Nd$ ratio of 0.7219. Repeated analyses of the La Jolla standard gave a $^{143}Nd/^{144}Nd$ ratio of 0.511867 ± 0.000018 (2SD, n = 12) in agreement with the recommended value of 0.511858 (Lugmair et al., 1983). Nd isotopes are reported using the εNd notation, normalising samples to the Chondritic Uniform Reservoir (CHUR) value of $^{143}Nd/^{144}Nd = 0.512638$; (Jacobsen and Wasserburg, 1980):

$$\varepsilon Nd = \left(\frac{(^{143}Nd/^{144}Nd)_{measured}}{(^{143}Nd/^{144}Nd)_{CHUR}} - 1\right) * 10^4 \quad (1)$$

Sr isotope ratios were measured in dynamic mode, corrected for instrumental mass bias using $^{87}Sr/^{86}Sr = 0.1194$. Repeated analyses of the NBS 987 standard gave a $^{87}Sr/^{86}Sr$ ratio of 0.710231 ± 0.000032 (2SD, n = 15) in agreement with the recommended value of Hodell et al. (2007) (0.710240). Blank contributions for Nd and Sr were assessed by ICP-MS and found to be negligible (< 1 per mil).

3.3. Elemental ratios diagnostics

Post-Archaean average Australian shale values (PAAS) were used for normalisation of major and selected trace element data in spider diagrams and rare earth element plots; (Pourmand et al., 2012). In order to minimize the effect of possible bias in absolute concentrations the concentrations in samples where normalised by the corresponding Al_2O_3 concentrations and these ratios were normalized against the $[X]_{PAAS}/[Al_2O_3]_{PAAS}$ ratio where $[X]_{PAAS}$ and $[Al_2O_3]_{PAAS}$ represent the concentrations of X and Al_2O_3 for PAAS.

Europium anomalies (Eu/Eu*) were calculated according to the following equation:

$$Eu/Eu* = Eu_N/(Sm_N + Gd_N)/2 \quad (2)$$

where N refers to PAAS-normalized values (Pourmand et al., 2012)

The Al/Si ratio has been shown to be dependent upon particle size in the Amazon Basin. Vertical gradients of the grain-size parameter D < 90 μm and Al/Si in the water column are inversely correlated (Bouchez et al., 2011).

The Th/Sc ratio is usually taken as an indicator for igneous differentiation processes (McLennan et al., 1993), while Cr/Th ratio can be used to discriminate between "basic" and "silicic" sediments (Cullers, 2000). Fine-grained sediments derived from basic rock sources typically have Th/Sc ratios lower than 0.4 and Cr/Th higher than 22. In contrast, fine grained sediments derived from more acidic rock sources display Th/Sc ratios higher than 0.64 and Cr/Th ratios lower than 15 (Cullers, 2000).

The Chemical Index of Alteration (CIA) measures the degree of feldspar weathering and the depletion of Na^+, K^+ and Ca^{2+} relative to Al, which remains immobile in secondary weathered products (Nesbitt and Young, 1982). It is defined as follows:

$$CIA = [Al_2O_3/(Al_2O_3 + CaO* + Na_2O + K_2O)] \times 100 \text{ (molar unit)} \quad (3)$$

where CaO* represents the CaO content in the silicate fraction.

CIA values for unaltered plagioclase and K-feldspars are approximately equal to 50, while sediments with substantial amounts of aluminous clay minerals (such as kaolinite) generally display higher CIA values (between 80 and 100) (Nesbitt and Young, 1982).

4. Results

4.1. River discharge and SPM variations

The Amazon is characterized by maximum and minimum discharges from March to July and October to January, respectively (Fig. 3a). During the sampling period, the Amazon discharge ranged from 76,500 $m^3 \cdot s^{-1}$ to 260,000 $m^3 \cdot s^{-1}$, while SPM concentrations varied from 8 $mg \cdot l^{-1}$ (July 2012) to 160 $mg \cdot l^{-1}$ (January 2013), increasing together with discharge in December and then decreasing during sustained high water discharge. The water discharge vs SPM concentration exhibits a clockwise hysteresis behaviour (Martinez et al., 2009).

The Orinoco River exhibits a low water stage from February to April and a high water stage in August (Fig. 3B; Laraque et al., 2013b). In 2008, the Orinoco River discharge ranged from 4700 $m^3 \cdot s^{-1}$ in April to 7040 $m^3 \cdot s^{-1}$ in August. SPM concentrations were minimal in April during the low discharge period (10 $mg \cdot l^{-1}$) and maximal in June during the rise of water discharge (160 $mg \cdot l^{-1}$). Another SPM maximum (98 $mg \cdot l^{-1}$) occurred in December, as documented in previous studies (Laraque et al., 2013b; Mora et al., 2014).

During the 2008 hydrological cycle, the Maroni River discharge ranged from 280 $m^3 \cdot s^{-1}$ in November to 7010 $m^3 \cdot s^{-1}$ in June (Fig. 3C). The highest (36 $mg \cdot l^{-1}$) and lowest (7 $mg \cdot l^{-1}$) SPM concentrations were observed in February and November, respectively, during the periods of high and low water discharges.

4.2. Mineralogy

Quartz, mica + illite and kaolinite contents are expressed as a semi-quantitative relative frequency of integrated XRD signals (Table 1). To a first order, SPM from the Amazon and Orinoco Rivers exhibit similar mineral proportions (Fig. 4a). In detail, Amazon SPM are slightly depleted in kaolinite and more enriched in mica + illite compared to those of Orinoco. In contrast, the Maroni SPM are almost exclusively composed of kaolinite (Fig. 4a). While there is no significant correlation between mineralogical composition and river discharge in the Maroni ($R^2 < 0.42$), the relative abundances of quartz in samples from the Amazon and the Orinoco Rivers (between 20 and 60%) display a

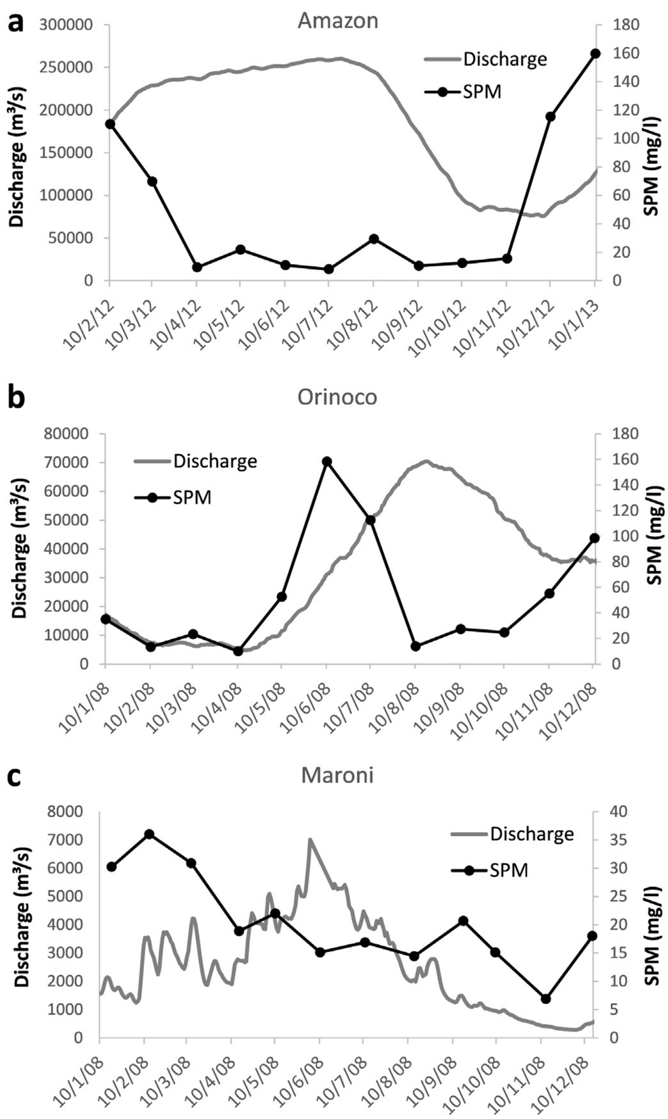

Fig. 3. Daily discharge (Hybam website) and suspended particulate matter (SPM) concentrations sampled once a month for the Amazon, Orinoco and Maroni Rivers during the periods covered in this study.

significant correlation with SPM concentrations: $R^2 = 0.87$; N = 12; p-value < 0.01, and $R^2 = 0.79$; N = 11; p-value < 0.01, respectively (Fig. 4b).

4.3. Major, minor and selected trace elements

Amazon and Orinoco SPM display very similar PAAS-normalized patterns characterized by relative depletions in TiO_2, MgO, Na_2O, K_2O, Rb, Cs, Zr, Nb Cr and Co (Figs. 5a, b). In detail, Orinoco SPM display higher relative abundances of MgO, CaO, Na_2O, Ba and Sr and lower relative abundances of FeO, Th, U, Y, Zr and Hf. In contrast, Maroni SPM (Fig. 5c) have similar relative abundances in TiO_2, FeO, MnO, Sc and V as those of the Amazon and Orinoco SPM, but are depleted in SiO_2 and the differences between mobile and refractory elements are exacerbated (Fig. 5d).

In this study, the Amazon and Orinoco SPM (which correspond to particles from surface waters) display quite similar Al/Si atomic ratios (mean ~0.47 ± 0.05 and 0.40 ± 0.04 respectively) (Table 2). These Al/Si ratios are much lower than those of the Maroni SPM (~ 0.8 ± 0.04) suggesting that the Amazon and Orinoco exhibit higher mean SPM grain size.

Orinoco SPM showed the highest Th/Sc ratios (0.72–0.97, mean ~0.85) and lowest Cr/Th ratios (4.5–7, mean ~5.3) (Table 2). For the Amazon SPM, Th/Sc and Cr/Th ratios showed intermediate values (Th/Sc: 0.33–0.76, mean; ~0.64 and Cr/Th: 5.3–7.5, mean ~6.0), while Maroni SPM, except for one anomalous sample (MAR06, June), showed overall lower Th/Sc ratios (0.41–1.25, mean ~0.60) and higher Cr/Th ratios (4.7–18.8, mean ~12.3).

For CIA calculations, neither carbonate leaching nor CO_2 analyses were conducted on our samples, so direct correction of carbonate--bound Ca in the studied SPM cannot be quantified. However, based on our mineralogical analyses and previous evidence from Bouchez et al. (2011), we expect the contribution of solid carbonate phases to be negligible at the studied stations, mostly because carbonate-rich sediments issued from the Andes are thought to be rapidly dissolved during river transport. The CIA values for Amazon SPM range from 68 (OB9, September) to 79 (OB13, January). For the Orinoco SPM, CIA values range from 77 (ORI7, July) to 83 (ORI4). The Maroni SPM have the highest CIA values ranging from 87 (MAR4) to 95 (MAR6) (Table 2). Considering the whole dataset the CIA values are negatively correlated with the mica + illite content ($R^2 = -0.83$).

4.4. Rare earth elements (REE)

REE concentrations are reported in Table 3 and PAAS-normalised REE patterns in Fig. 6. Amazon SPM display a slight MREE enrichment (Gd/Nd = 1.04 ± 0.09), whereas Orinoco SPM presents a relatively flat pattern. These results are similar to that found by Bayon et al. (2015) for the Amazon and Orinoco clay-size fractions. Maroni SPM presents a LREE enrichment over HREE (Nd/Yb = 1.36 ± 0.19). Orinoco, Maroni and Amazon SPM can be distinguished based on their Eu anomalies. The Maroni SPM have the highest Eu/Eu* ratios (1.40–1.64, mean~1.51). The Amazon SPM have Eu/Eu* ratios (1.16–1.39, mean ~1.24) higher than those of the Orinoco (1.03–1.23, mean ~1.14). Calculated Eu/Eu* ratios for the Amazon and Orinoco clay based on Bayon et al. (2015) dataset yield similar Eu/Eu* ratios (1.20 and 1.07 respectively).

4.5. Nd and Sr isotopic compositions

Amazon SPM exhibit εNd values ranging from −9.8 (OB11, November) to −11.4 (OB6, June), with $^{87}Sr/^{86}Sr$ ratios varying from 0.7173 (OB10, September) to 0.7266 (OB3, March) (Table 3). Compared to the Amazon SPM, the Orinoco SPM display less radiogenic Nd isotopic signatures, with εNd values ranging from −13.7 (ORI01 and ORI03 January and March respectively) to −14.6 (ORI09, August), and more radiogenic $^{87}Sr/^{86}Sr$ ratios, with values ranging between 0.7257 (ORI03, March) and 0.7306 (ORI11, November). In contrast, the Maroni SPM are characterized by much lower Nd isotopic compositions with εNd values ranging from −21 (MAR04, April) to −25.2 (MAR06, June) and slightly higher $^{87}Sr/^{86}Sr$ ratios, with values ranging between 0.72954 (MAR04, April) and 0.73611 (MAR03, March). The Sr isotopic composition of analysed SPM rivers show a strong negative correlation with the mica + illite content ($R^2 = -0.81$, Fig. 7).

5. Discussion

The Amazon, Orinoco and Maroni SPM are characterized by distinct mineralogical compositions, major and trace element concentrations, Al/Si, Eu/Eu*, Cr/Th, Th/Sc ratios and Sr−Nd isotopic compositions (Figs. 4–7 and Tables 1–3).

Before drawing conclusions on the relative influence of source rock composition and hydrological cycle on the geochemical composition of the SPM, the effect of chemical weathering and grain size sorting must be carefully evaluated as it may control the REE contents and radiogenic isotopes composition of the SPM (Bouchez et al., 2011; Bayon et al., 2015).

Table 1
Date and location of suspended particulate matter (SPM) sampling of the Amazon, Orinoco and the Maroni Rivers and corresponding discharges, SPM concentration and relative mineralogical composition.

Sample	Month	Date	Discharge[a]	SPM	Mica Illite	Kaolinite	Quartz
			$m^3 \cdot s^{-1}$	$mg \cdot l^{-1}$	Rel. int %	Rel. int %	Rel. int %
Amazon at Óbidos (01.9225°S; 55.6753°)							
OB 02	Feb	10/02/12	195,900	110.2	0.25	0.22	0.53
OB 03	Mar	10/03/12	231,000	69.8	0.27	0.19	0.54
OB 04	Apr	10/04/12	240,200	9.3	0.38	0.32	0.29
OB 05	May	10/05/12	247,600	21.8	0.30	0.33	0.37
OB 06	Jun	10/06/12	254,500	10.9	0.37	0.33	0.30
OB 07	Jul	10/07/12	258,300	8.0	0.39	0.34	0.27
OB 08	Aug	10/08/12	231,200	29.3	0.28	0.26	0.47
OB 09	Sep	10/09/12	157,100	10.4	0.41	0.38	0.21
OB10	Oct	10/10/12	93,460	12.4	0.35	0.39	0.26
OB11	Nov	10/11/12	80,860	15.6	0.36	0.43	0.21
OB12	Dec	10/12/12	90,490	115.3	0.26	0.19	0.56
OB13	Jan	10/01/13	133,600	159.7	nd	nd	nd
Orinoco at Ciudad bolivar (08.1536° N; 063.5361°W)							
ORI 01	Jan	10/01/08	14,760	34.9	0.24	0.30	0.45
ORI 02	Feb	10/02/08	7469	13.3	0.30	0.41	0.29
ORI 03	Mar	10/03/08	6856	23.3	0.29	0.44	0.27
ORI 04	Apr	10/04/08	5959	10.0	0.29	0.46	0.25
ORI 05	May	10/05/08	15,090	52.7	0.25	0.48	0.27
ORI 06	Jun	10/06/08	33,720	158.2	nd	nd	nd
ORI 07	Jul	10/07/08	53,970	112.4	0.17	0.23	0.60
ORI 08	Aug	10/08/08	68,530	13.8	0.30	0.42	0.28
ORI 09	Sep	10/09/08	62,900	27.3	0.27	0.33	0.40
ORI 10	Oct	10/10/08	48,600	24.7	0.26	0.36	0.39
ORI 11	Nov	10/11/08	36,890	55.1	0.22	0.28	0.50
ORI 12	Dec	11/12/08	32,530	98.4	nd	nd	nd
Maroni at Langa Tabiki (05.1401° S; 054.3551° W)							
MAR 01	Jan	18/01/08	1784	30.2	0.08	0.90	0.02
MAR 02	Feb	13/02/08	2763	36.0	0.10	0.85	0.05
MAR 03	Mar	13/03/08	2840	30.9	0.09	0.87	0.04
MAR 04	Apr	15/04/08	2929	18.9	0.14	0.80	0.07
MAR 05	May	10/05/08	4486	22.0	0.07	0.90	0.03
MAR 06	Jun	10/06/08	nd	15.1	0.08	0.90	0.02
MAR 07	Jul	11/07/08	3939	16.9	0.09	0.89	0.02
MAR 08	Aug	14/08/08	2421	14.4	0.08	0.87	0.05
MAR 09	Sep	17/09/08	1333	20.7	0.10	0.89	0.01
MAR 10	Oct	09/10/08	854.3	15.1	0.08	0.88	0.04
MAR 11	Nov	13/11/08	402.5	6.9	0.12	0.83	0.05
MAR 12	Dec	15/12/08	598.4	18.0	0.17	0.77	0.06

[a] Discharges are expressed as monthly average values, Daily discharge values are accessible on Hybam website.

The CIA values of the Maroni SPM are substantially higher than those of the Orinoco and Amazon Rivers SPM. In addition, despite a slight overlap (Fig. 7), our data shows that the Orinoco SPM have higher CIA values than Amazon SPM (*t*-Test with $P < 0.05$). The Amazon CIA values calculated in this study (68–79) are similar to those calculated for Óbidos surface samples based on the dataset of Bouchez et al. (2011) (CIA = 70 to 77). The contrasts in CIA between the 3 basins could relate to differences in climatic conditions or differences in source rock composition. The Amazon, Orinoco and Maroni river basins are characterized by similar warm and wet climatic conditions, with respective mean annual temperatures of 26.7 °C, 23.9 °C and 26.5 °C, and mean annual precipitation of 2030 $mm \cdot y^{-1}$, 1400 $mm \cdot y^{-1}$ and 2520 $mm \cdot y^{-1}$ (Bayon et al., 2016; Sondag et al., 2010). Hence, difference in climatic condition is unlikely to account for both changes in rock weathering intensity and observed variations in the mineralogy and geochemistry of SPM from these river systems.

In addition to climate, grain-size heterogeneity due to hydrological sorting processes in the water column can also lead to geochemical variations between SPM from the investigated tropical South American rivers. As previously shown for the Amazon River (i.e. Bouchez et al., 2011), grain-size of the SPM increases with water depth at Óbidos as Al/Si ratios decreases from surface waters (~0.42) to deeper waters (0.21 at 55 m water depth) and bedload sediments (0.08). Our results show that grain size is quite similar for Amazon and Orinoco SPM and present a low annual variability with Al/Si standard deviations lower than 10%. Based on Al/Si ratios and kaolinite content, Maroni SPM are significantly finer and have also a lower annual variability (Al/Si standard deviation lower than 5%; Fig. 7). In addition, despite a slight correlation between Al/Si and Eu/Eu* for the Amazon ($R^2 = 0.51$; N = 12; p-value < 0.01) no correlation between Al/Si ratios and Eu/Eu*, Cr/Th, Th/Sc and Sr–Nd isotopic compositions of SPM is observed in the three basins. As we observe low variations in surface Al/Si ratios, no correlation with other variables and previous works showed no significant variations in SPM diameter during the hydrological cycle (Armijos et al., 2017; Bouchez et al., 2011; Pinet et al., 2017), we suggest that the observed mineralogical and geochemical differences are more likely to be controlled by differences in source rock lithology and variations of sedimentary fluxes during the hydrological cycle.

5.1. Source rock lithology

5.1.1. Maroni River

The Maroni River drains the old weathered Paleoproterozoic terranes of the Guyana shield. Similar igneous/metamorphic terranes from the Guyana shield are also drained by a series of right-bank tributaries of the Orinoco (Aro, Caroni and Caura Rivers) that were recently

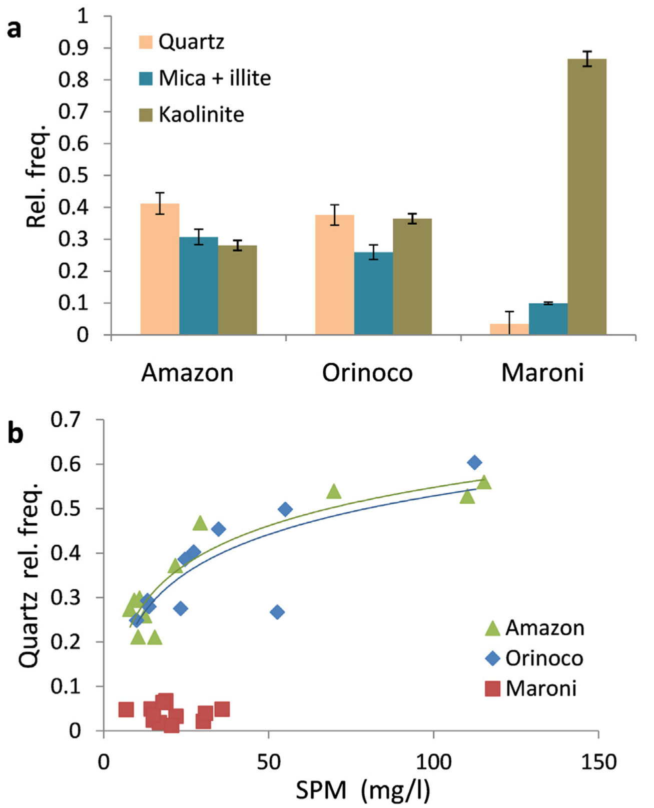

Fig. 4. a) Semi quantitative mineralogical compositions of Amazon, Orinoco and Maroni SPM expressed relative frequency of integrated XRD peaks signals and annually averaged for each river. b) Quartz content versus SPM concentration plot (logarithmic fitting for Amazon and Orinoco are also represented.)

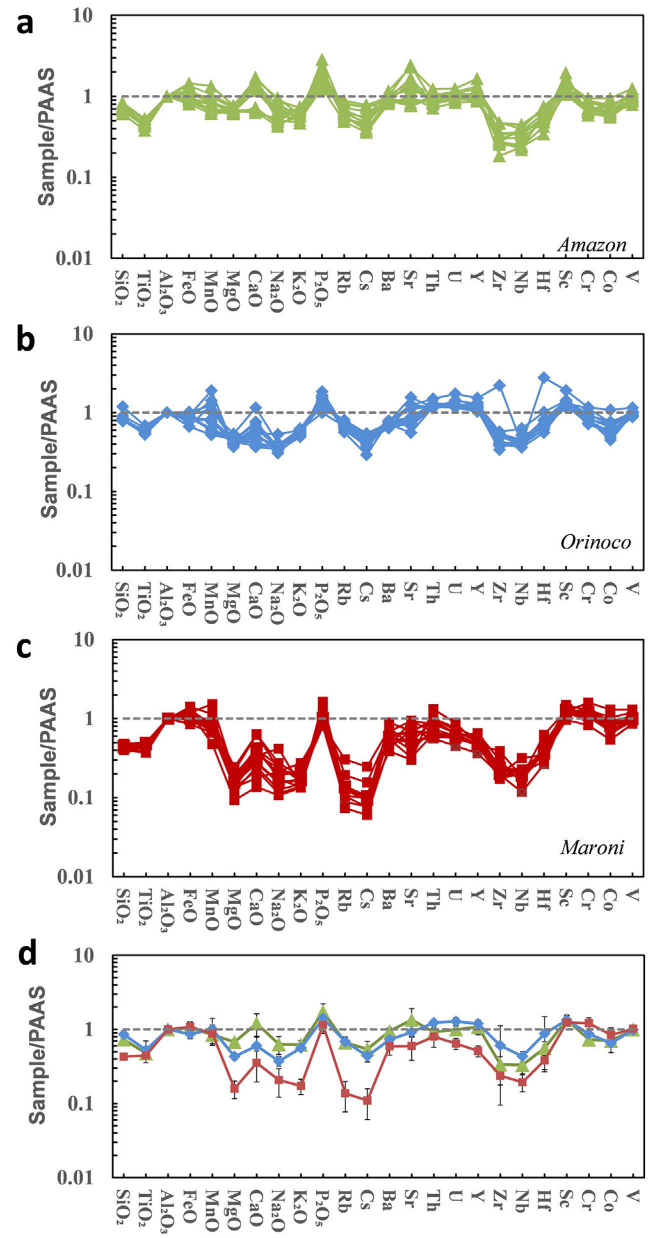

Fig. 5. Major and selected trace element compositions of Amazon, Orinoco and Maroni SPM normalized to PAAS (Pourmand et al., 2012) and corrected with $[Al_2O_3]_{PAAS}/[Al_2O_3]_{Sample\ ratios}$. From the left to the right abscissa of the diagram are plotted major elements (SiO_2, Al_2O_3, MnO, MgO, CaO, Na_2O, K_2O, TiO_2, P_2O_5), large ion lithophile elements (LILE) (Rb, Ba, Cs, Sr, Th and U), high field strength elements (HFSE) (Zr, Hf, Y and Nb), and transition trace elements (TTE) (Cr, Ci, V).

analysed by Bayon et al. (2015). Both these sediments analysed by Bayon et al. (2015) and the Maroni SPM are dominated by kaolinite (Figs. 3 and 6). A $^{87}Sr/^{86}Sr$ vs. εNd diagram comparing our data with other relevant data from the literature is presented in Fig. 8. These reference data include various volcanic and sedimentary rocks from the Andes (Barragan et al., 1998; Kay et al., 1994; Pinto, 2003; Rogers and Hawkesworth, 1989) and modern suspended sediments from the Solimões, Madeira and Amazon Rivers (Bouchez et al., 2011; Viers et al., 2008). The Maroni SPM display distinctive Sr–Nd isotopic compositions compared to the Amazon and Orinoco SPM, characterized by much lower εNd values and more radiogenic Sr isotopic ratios (Fig. 8, Table 3). To the best of our knowledge, no Sr isotopic data exist for river sediments derived from the Guyana shield. However, the Sr isotopic compositions of the Maroni SPM fall within the range of values reported for the dissolved fraction of the Maroni River ($^{87}Sr/^{86}Sr$ = 0.721–0.734; Négrel and Lachassagne, 2000) and other cratonic rivers in Brazil and Venezuela (Rio Branco: $^{87}Sr/^{86}Sr$ = 0.726–0.735 and Venturi river: $^{87}Sr/^{86}Sr$ = 0.726–0.742; Edmond et al., 1995). In addition, Maroni SPM have higher Al/Si ratios and hence finer grain-size, lower Th/Sc ratios, higher Eu/Eu*, Cr/Th and CIA values. All these geochemical and isotopic characteristics indicate that the Maroni River is exporting less differentiated, older and more weathered detritus than those from other analysed tropical South American rivers SPM.

5.1.2. Orinoco River

The geochemical and isotopic characteristics of the Orinoco SPM result from the mixing of terrigenous matter delivered from both left- and right-bank tributaries. Left-bank tributaries of the Orinoco River drain various magmatic rocks and sedimentary formations from the Andes, the Caribbean Coastal Range in northern Venezuela and the lowland floodplain. Right-bank tributaries are associated with older and more intensively weathered rocks from the Precambrian Guyana shield. Consequently, the Orinoco SPM have CIA values lower than those of the Maroni and higher than those of the Amazon. The Th/Sc and Cr/Th ratios indicate that Orinoco SPM are in average the results of the erosion of slightly more differentiated material than Amazon and Maroni SPM. The Orinoco SPM have also distinctive Sr–Nd isotopic compositions (Fig. 9). While extensive datasets for dissolved $^{87}Sr/^{86}Sr$ have been reported earlier (Edmond et al., 1996; Edmond et al., 1995), the only $^{87}Sr/^{86}Sr$ isotopic data available for Orinoco sediments (0.7406 ± 0.0013, n = 5; (Parra et al., 1997) are significantly more radiogenic than the Orinoco SPM analysed here

Table 2
Major and trace elements concentrations; Al/Si, Cr/Th and Th/Sc ratios; and Chemical Index of Alteration (CIA) in SPM from the Amazon, Orinoco and Maroni Rivers.

Sample	SiO2	TiO_2	Al_2O_3	FeO	MnO	MgO	CaO	Na_2O	K_2O	P_2O_5	Rb	Cs	Ba	Sr	Th	U	Y	Zr	Nb	Hf	Sc	Cr	Co	V	Ni	Al/Si	Cr/Th	Th/Sc	CIA
	%	%	%	%	%	%	%	%	%	%	ppm	ppm	ppm	ppm	ppm	ppm	ppm	ppm	ppm	ppm	ppm	ppm	ppm	ppm	ppm				
Amazon at Óbidos																													
OB 02	30.23	0.31	11.20	3.83	0.05	0.87	0.53	0.35	1.55	0.13	78.4	6.48	347	98.6	7.93	1.86	15.9	57.8	5.00	1.99	11.7	43.0	8.48	81.2	21.6	0.42	5.43	0.68	77.7
OB 03	28.06	0.28	10.10	3.66	0.04	0.78	0.44	0.34	1.47	0.11	76.0	6.20	338	84.4	7.86	1.78	15.4	52.9	4.55	1.84	10.7	41.6	8.22	72.9	26.7	0.41	5.30	0.73	77.4
OB 04	9.32	0.11	4.24	1.38	0.02	0.35	0.47	0.26	0.49	0.06	22.8	1.53	146	108.9	2.82	0.65	5.7	13.3	0.94	0.72	5.5	21.1	3.63	38.8	53.0	0.52	7.47	0.51	70.0
OB 05	12.23	0.14	5.35	2.91	0.04	0.48	0.60	0.21	0.59	0.13	28.6	2.30	214	130.2	5.08	1.09	12.6	16.1	1.36	0.77	6.7	29.4	6.17	52.8	96.4	0.50	5.80	0.76	72.0
OB 06	9.14	0.10	3.94	2.01	0.02	0.35	0.40	0.17	0.54	0.08	20.3	1.49	142	61.0	3.18	0.74	7.5	15.5	1.38	0.58	4.7	19.8	3.62	34.4	28.6	0.49	6.23	0.67	71.3
OB 07	7.12	0.08	2.85	1.15	0.02	0.24	0.28	0.14	0.33	0.04	13.8	0.90	85	44.7	1.78	0.43	3.8	10.8	1.06	0.46	3.0	14.7	2.72	22.5	32.7	0.45	8.25	0.59	72.2
OB 08	17.48	0.18	6.32	2.86	0.03	0.51	0.57	0.25	0.82	0.10	36.3	2.58	218	81.3	4.77	1.11	11.4	33.3	2.52	1.25	7.0	25.4	5.93	49.3	53.4	0.41	5.34	0.68	73.0
OB 09	6.26	0.06	2.84	1.26	0.01	0.21	0.33	0.16	0.40	0.05	13.7	0.85	91	50.6	1.84	0.42	4.1	8.0	0.69	0.32	2.7	10.5	2.68	22.8	38.3	0.51	5.73	0.69	68.4
OB 10	19.58	0.19	8.14	2.86	0.04	0.60	0.66	0.31	0.81	0.09	33.7	2.29	227	85.8	4.50	1.12	10.1	27.5	2.52	1.04	13.4	27.8	6.07	51.1	72.9	0.47	6.17	0.33	75.9
OB 11	9.98	0.10	4.94	2.06	0.02	0.35	0.50	0.16	0.45	0.08	22.2	1.77	162	67.8	3.26	0.76	7.7	10.1	1.18	0.45	5.4	19.2	3.93	40.5	36.1	0.56	5.88	0.61	74.8
OB 12	26.00	0.26	10.43	3.14	0.04	0.78	0.47	0.28	1.30	0.11	71.8	5.96	317	84.4	7.58	1.59	13.4	39.8	3.52	1.46	10.6	38.1	7.01	72.2	17.2	0.45	5.03	0.71	79.3
OB 13	66.93	0.66	26.96	8.71	0.10	1.90	1.35	0.77	3.00	0.31	167.0	13.68	772	265.7	17.57	4.36	34.7	86.8	10.22	3.50	24.1	98.8	18.83	200.9	77.8	0.46	5.62	0.73	79.4
Orinoco at Ciudad bolivar																													
ORI 01	41.7	0.45	15.5	4.9	0.08	0.81	0.81	0.24	1.76	0.11	59.3	3.66	247	88.5	9.44	1.99	15.6	44.3	3.67	1.49	11.3	66.5	9.19	81.5	229.4	0.42	7.04	0.83	80.5
ORI 02	40.6	0.46	15.4	3.8	0.11	0.72	0.66	0.36	1.60	0.20	87.0	5.05	347	206.5	13.71	3.21	23.7	57.9	7.99	2.67	15.2	73.2	9.14	126.7	32.0	0.43	5.34	0.90	81.3
ORI 03	65.5	nd	23.1	7.4	0.19	1.09	0.89	0.45	2.45	0.18	96.2	6.06	381	122.4	15.65	3.28	25.4	74.7	6.69	2.64	16.6	79.4	12.89	125.5	115.1	0.40	5.07	0.94	82.2
ORI 04	45.3	0.48	17.1	5.9	0.19	0.73	0.64	0.36	1.65	0.18	63.1	4.01	250	89.5	11.60	2.34	19.1	51.5	4.53	1.85	11.9	54.6	9.93	88.3	72.8	0.43	4.71	0.97	82.9
ORI 05	39.4	0.36	10.0	2.5	0.03	0.53	0.38	0.33	1.17	0.08	56.5	2.79	262	164.6	8.86	2.34	18.2	63.0	6.29	2.68	11.9	46.1	6.82	78.4	104.4	0.29	5.21	0.74	79.9
ORI 06	53.9	0.55	19.3	6.3	0.07	0.96	0.51	0.46	2.33	0.13	85.7	5.53	329	79.1	12.22	2.56	19.8	73.0	5.51	2.49	13.9	57.4	8.74	93.9	31.2	0.41	4.70	0.88	82.1
ORI 07	41.1	0.46	13.6	5.1	0.08	0.85	1.08	0.36	1.32	0.19	64.9	3.10	369	178.5	15.82	3.88	29.8	335.4	5.47	10.02	22.1	92.5	17.97	124.7	693.2	0.38	5.85	0.72	77.4
ORI 08	28.6	0.33	11.0	4.2	0.08	0.53	0.49	0.26	1.19	0.15	59.8	3.46	288	90.9	9.83	2.21	21.1	46.3	4.43	1.79	12.3	59.6	10.23	85.9	76.7	0.44	6.07	0.80	80.8
ORI 09	35.4	0.41	13.0	4.7	0.08	0.67	0.64	0.30	1.31	0.18	66.5	3.82	343	120.3	13.15	2.70	22.7	75.9	5.65	2.31	15.7	71.2	11.32	105.7	150.9	0.42	5.42	0.84	80.9
ORI 10	26.0	0.29	9.5	2.8	0.05	0.44	0.32	0.23	1.14	0.11	58.3	3.51	258	112.7	8.95	1.91	17.2	56.8	4.23	2.03	11.2	46.5	5.20	75.1	10.0	0.42	5.20	0.80	81.2
ORI 11	43.3	0.47	15.5	5.2	0.07	0.78	0.45	0.34	1.81	0.16	98.4	6.07	402	117.5	14.38	3.09	25.5	90.5	6.20	3.24	16.6	64.7	11.28	113.4	50.4	0.40	4.50	0.87	82.2
ORI 12	37.0	0.37	13.4	4.4	0.05	0.70	0.34	0.29	1.64	0.14	91.0	5.69	339	96.3	12.02	2.60	20.7	72.5	5.68	2.56	14.1	55.7	9.05	96.2	34.3	0.41	4.63	0.85	82.4
Maroni at Langa Tabiki																													
MAR 01	9.8	0.18	7.1	2.3	0.04	0.12	0.17	0.11	0.25	0.05	5.32	0.43	103	54.1	3.08	0.53	3.7	15.4	0.84	0.50	7.5	50.3	5.61	52.5	3.9	0.82	16.30	0.41	90.3
MAR 02	18.7	0.31	12.4	4.8	0.05	0.22	0.24	0.12	0.40	0.09	14.45	1.01	243	66.6	5.72	1.19	8.5	27.3	2.36	1.18	13.5	86.9	12.65	99.2	37.5	0.75	15.18	0.42	92.0
MAR 03	10.8	0.19	7.5	2.8	0.04	0.13	0.20	0.09	0.31	0.06	8.57	0.55	151	54.6	3.78	0.73	5.1	19.9	1.49	0.75	7.8	48.6	7.33	58.0	41.3	0.79	12.86	0.49	89.7
MAR 04	10.6	0.18	6.6	2.7	0.03	0.19	0.29	0.11	0.25	0.07	10.81	0.81	156	65.8	3.42	0.65	6.1	17.4	1.12	0.65	8.3	48.6	7.46	53.9	57.2	0.71	14.20	0.41	87.1
MAR 05	9.0	0.16	6.6	2.4	0.04	0.17	0.28	0.10	0.25	0.07	4.11	0.31	102	64.8	4.35	0.71	4.4	12.6	1.35	0.51	6.5	37.7	7.80	46.4	76.8	0.82	8.67	0.67	87.5
MAR 06	17.7	0.31	13.3	5.9	0.04	0.14	0.12	0.09	0.35	0.16	12.03	1.02	176	42.6	13.54	1.93	8.9	29.6	4.24	1.22	10.8	64.0	8.74	90.9	40.8	0.85	4.73	1.25	94.6
MAR 07	23.0	0.40	16.9	8.2	0.08	0.26	0.39	0.45	0.47	0.23	17.57	1.42	325	88.2	12.89	1.98	12.1	43.7	3.88	1.69	16.6	103.9	14.25	136.8	41.1	0.83	8.06	0.78	89.6
MAR 08	25.3	0.44	17.2	9.1	0.11	0.35	0.52	0.19	0.46	0.21	18.08	1.38	376	122.4	13.36	2.16	14.2	46.1	2.98	1.80	21.2	129.4	21.82	162.8	116.6	0.77	9.69	0.63	90.8
MAR 09	45.8	0.69	31.5	11.7	0.13	0.48	0.49	0.23	0.86	0.27	35.09	2.51	594	107.7	15.57	2.90	20.9	94.6	6.12	3.42	31.8	203.3	28.19	232.1	113.5	0.78	13.06	0.49	93.5
MAR 10	25.9	0.40	18.1	7.7	0.10	0.25	0.31	0.15	0.53	0.16	15.92	1.09	376	77.3	10.36	1.79	17.0	59.9	2.81	2.28	18.9	136.9	20.55	155.5	157.1	0.79	13.22	0.55	93.0
MAR 11	4.2	0.06	3.2	1.4	0.03	0.07	0.09	0.05	0.10	0.03	3.38	0.23	98	23.3	2.29	0.34	2.6	6.3	nd	0.25	3.3	29.5	5.02	32.8	20.2	0.85	12.91	0.69	90.0
MAR 12	33.3	0.45	22.9	7.3	0.09	0.36	0.28	0.31	1.23	0.16	59.16	4.42	591	114.1	11.10	2.47	15.3	98.8	4.23	3.79	24.7	209.2	18.75	187.9	131.7	0.78	18.84	0.45	90.7
GA Standard																													
Average	68.72	0.24	14.56	2.36	0.08	0.84	2.28	3.46	3.71	0.13	149.5	5.5	792	290	14.8	5.1	17.3	97.1	3.58	3.19	10.18	11.7	4.02	38.8	9.8				
2Sd(n = 3)	1.13	0.00	0.17	0.18	0.01	0.06	0.04	0.04	0.04	0.01	4.9	0.3	3	7	0.2	2	1.0	33.2	1.83	1.17	0.34	7.3	0.67	1.7	11.8				
Compiled[a]	69.9	0.38	14.5	2.27	0.09	0.95	2.45	3.45	3.18	0.12	175	6	840	310	17	5	21	150	12	4	7	12	5	38	7				

[a] GA standard values reported for comparison are from (Abbey, 1980).

Table 3
REE concentrations and Nd–Sr isotopic of SPM from the Amazon, Orinoco and Maroni Rivers.

Sample	La	Ce	Pr	Nd	Sm	Eu	Gd	Tb	Dy	Ho	Er	Tm	Yb	Lu	$\frac{Eu_n}{Eu*}$	$\frac{Nd_n}{Yb_n}$	$\frac{Gd_n}{Yb_n}$	$\frac{Gd_n}{Nd_n}$	$\frac{^{143}Nd}{^{144}Nd}$	2SEM	$\varepsilon Nd_{(0)}$	+/−	$\frac{^{87}Sr}{^{86}Sr}$	2SEM
	ppm	ppm	ppm	ppm	ppm	ppm	ppm	ppm	ppm	ppm	ppm	ppm	ppm	ppm										
Amazon at Óbidos																								
OB 02	28.0	50.28	6.44	23.37	4.68	0.947	3.59	0.578	3.25	0.66	1.97	0.270	1.66	0.26	1.22	1.14	1.08	0.95	0.512089	0.000004	−10.7	0.08	0.723245	0.000009
OB 03	23.9	47.65	6.06	22.14	4.44	0.901	3.52	0.551	3.16	0.64	1.89	0.258	1.58	0.25	1.21	1.13	1.11	0.98	0.512067	0.000005	−11.1	0.10	0.726616	0.000009
OB 04	8.8	18.90	2.56	9.38	1.74	0.408	1.40	0.221	1.22	0.29	0.75	0.106	0.61	0.11	1.39	1.25	1.15	0.92	0.512054	0.000007	−11.4	0.14	0.720084	0.000008
OB 05	43.0	32.16	4.56	16.65	3.61	0.783	3.23	0.481	2.55	0.52	1.53	0.196	1.23	0.18	1.22	1.09	1.30	1.20	0.512079	0.000015	−10.9	0.29	0.723671	0.000018
OB 06	11.0	20.95	3.04	11.35	2.42	0.529	1.96	0.307	1.58	0.33	0.88	0.128	0.70	0.10	1.29	1.31	1.40	1.07	0.512053	0.000007	−11.4	0.14	0.721621	0.000014
OB 07	5.9	11.25	1.49	5.37	1.14	0.226	0.93	0.144	0.80	0.17	0.49	0.070	0.39	0.07	1.16	1.10	1.17	1.07	0.512101	0.000008	−10.5	0.16	0.717838	0.000020
OB 08	15.3	30.55	4.08	14.73	3.02	0.634	2.55	0.411	2.21	0.46	1.38	0.202	1.06	0.17	1.21	1.12	1.20	1.07	0.512090	0.000005	−10.7	0.10	0.720094	0.000009
OB 09	6.8	11.99	1.58	5.82	1.24	0.280	1.04	0.165	0.86	0.18	0.51	0.076	0.39	0.07	1.31	1.22	1.34	1.10	0.512087	0.000009	−10.7	0.18	0.718524	0.000012
OB 10	15.7	30.15	3.92	14.19	2.82	0.590	2.30	0.378	2.03	0.42	1.21	0.160	1.06	0.15	1.23	1.08	1.08	1.00	0.512098	0.000007	−10.5	0.14	0.717343	0.000010
OB 11	12.1	22.67	2.94	10.85	2.26	0.520	1.96	0.303	1.57	0.33	0.91	0.126	0.72	0.12	1.31	1.21	1.35	1.12	0.512134	0.000009	−9.8	0.18	0.718239	0.000008
OB 12	22.5	45.41	5.70	20.83	4.21	0.816	3.12	0.508	2.84	0.58	1.71	0.237	1.47	0.22	1.19	1.14	1.06	0.92	0.512135	0.000007	−9.8	0.14	0.724153	0.000064
OB 13	59.7	114.02	14.24	51.73	10.62	2.217	9.31	1.312	7.02	1.46	4.42	0.619	3.88	0.58	1.18	1.08	1.20	1.11	0.512137	0.000008	−9.8	0.16	0.723868	0.000011
Orinoco at Ciudad bolivar																								
ORI 01	28.2	56.3	7.14	24.5	4.80	0.903	3.41	0.538	3.30	0.651	1.86	0.296	1.75	0.272	1.18	1.13	0.97	0.86	0.511934	0.000009	−13.7	0.18	0.727706	0.000010
ORI 02	44.4	89.3	10.93	38.6	7.34	1.459	5.36	0.826	4.66	1.057	2.99	0.444	2.55	0.418	1.23	1.22	1.05	0.86	0.511907	0.000030	−14.3	0.58	0.726018	0.000011
ORI 03	45.8	94.6	11.50	40.1	7.87	1.487	5.60	0.842	5.26	1.035	3.06	0.421	2.72	0.441	1.18	1.19	1.02	0.86	0.511935	0.000006	−13.7	0.12	0.725650	0.000008
ORI 04	34.2	70.5	8.58	30.6	5.96	1.086	4.43	0.663	3.90	0.793	2.23	0.326	1.92	0.335	1.12	1.29	1.15	0.89	0.511905	0.000012	−14.3	0.23	0.727609	0.000023
ORI 05	35.0	57.9	7.28	25.7	4.96	0.945	3.76	0.599	3.59	0.791	2.20	0.371	2.05	0.330	1.16	1.01	0.91	0.90	nd	nd	nd	nd	nd	nd
ORI 06	34.7	67.6	8.25	29.0	5.89	1.073	4.31	0.679	4.04	0.759	2.23	0.317	2.12	0.322	1.13	1.10	1.01	0.92	0.511912	0.000008	−14.2	0.16	0.730289	0.000012
ORI 07	55.3	100.6	12.55	43.4	8.67	1.514	6.30	0.944	5.94	1.236	3.40	0.583	3.51	0.574	1.08	1.00	0.90	0.90	0.51191	0.000010	−14.2	0.19	0.730062	0.000012
ORI 08	33.4	69.7	8.52	30.0	6.09	1.147	4.76	0.768	4.39	0.856	2.30	0.358	2.22	0.345	1.13	1.09	1.07	0.98	0.511892	0.000008	−14.6	0.16	0.730224	0.000010
ORI 09	52.6	79.2	9.88	34.8	6.74	1.268	5.17	0.794	4.78	0.905	2.55	0.402	2.53	0.411	1.14	1.11	1.02	0.92	0.511931	0.000004	−13.8	0.08	0.729280	0.000010
ORI 10	26.4	51.9	6.58	22.9	4.55	0.908	3.49	0.553	3.28	0.655	1.91	0.300	1.70	0.304	1.21	1.09	1.02	0.94	0.511922	0.000009	−14.0	0.18	0.729615	0.000017
ORI 11	40.1	80.2	10.07	36.0	6.95	1.321	5.42	0.859	5.27	1.025	3.15	0.473	2.91	0.431	1.14	1.00	0.93	0.93	0.511918	0.000005	−14.0	0.10	0.730605	0.000012
ORI 12	34.8	67.8	8.41	30.4	5.76	1.137	4.49	0.701	4.33	0.832	2.50	0.364	2.38	0.340	1.19	1.03	0.94	0.91	0.511926	0.000004	−13.9	0.08	0.730068	0.000010
Maroni at Langa Tabiki																								
MAR 01	74.5	17.7	2.02	7.0	1.29	0.334	1.04	0.139	0.84	0.151	0.44	0.066	0.41	0.070	1.53	1.40	1.28	0.91	0.511387	0.000006	−24.4	0.12	0.732866	0.000011
MAR 02	20.6	34.7	4.07	14.3	2.65	0.669	2.10	0.32	1.81	0.366	1.00	0.155	0.87	0.149	1.50	1.32	1.20	0.91	0.511459	0.000008	−23.0	0.16	0.736056	0.000011
MAR 03	13.2	22.9	2.65	9.2	1.71	0.452	1.23	0.189	1.15	0.221	0.62	0.089	0.59	0.092	1.64	1.25	1.04	0.83	0.511411	0.000010	−23.9	0.19	0.736110	0.000015
MAR 04	12.9	22.2	2.67	9.1	1.80	0.465	1.51	0.201	1.31	0.253	0.66	0.111	0.59	0.115	1.50	1.23	1.27	1.03	0.511551	0.000006	−21.2	0.12	0.729543	0.000009
MAR 05	14.0	23.1	2.54	8.6	1.66	0.390	1.09	0.175	1.02	0.193	0.53	0.083	0.44	0.076	1.53	1.58	1.23	0.78	0.511362	0.000007	−24.9	0.14	0.731574	0.000009
MAR 06	46.4	54.9	5.77	19.3	3.52	0.779	2.44	0.369	1.96	0.393	1.01	0.152	0.90	0.136	1.40	1.73	1.35	0.78	0.511346	0.000007	−25.2	0.14	0.733496	0.000009
MAR 07	30.0	64.1	6.78	24.5	4.41	1.013	2.97	0.492	2.62	0.531	1.34	0.206	1.28	0.202	1.47	1.54	1.16	0.75	0.511381	0.000010	−24.5	0.19	0.733396	0.000008
MAR 08	42.3	72.8	8.21	27.8	5.23	1.172	3.44	0.59	3.22	0.689	1.76	0.272	1.60	0.240	1.45	1.40	1.07	0.76	0.511389	0.000011	−24.4	0.21	0.733831	0.000010
MAR 09	46.5	91.8	10.63	37.4	6.85	1.726	5.37	0.782	4.48	0.843	2.44	0.360	2.35	0.358	1.51	1.28	1.14	0.89	0.511456	0.000011	−23.1	0.21	0.735659	0.000009
MAR 10	31.6	60.5	6.84	23.9	4.41	1.079	3.27	0.519	2.81	0.575	1.45	0.223	1.56	0.208	1.50	1.24	1.05	0.85	0.511447	0.000010	−23.2	0.19	0.733624	0.000010
MAR 11	6.6	12.6	1.40	5.0	0.98	0.244	0.62	0.108	0.56	0.121	0.33	0.050	0.30	0.050	1.64	1.33	1.02	0.77	0.51139	0.000006	−24.3	0.12	0.733216	0.000016
MAR 12	36.1	66.0	7.56	27.0	5.14	1.244	3.72	0.575	3.33	0.659	1.89	0.312	2.16	0.333	1.50	1.01	0.86	0.85	0.511505	0.000011	−22.1	0.21	0.732296	0.000017
GA Standard																								
Average	36.19	66.04	7.59	25.23	4.74	0.98	3.43	0.56	3.33	0.66	1.86	0.29	1.92	0.30										
2Sd(n = 3)	10.19	12.15	1.38	3.46	0.54	0.05	0.12	0.04	0.27	0.04	0.15	0.03	0.28	0.03										
Compiled[a]	40	76	8.3	27	5	1.08	3.8	0.6	3.3	0.7	2	0.3	2	0.3										

[a] GA standard values reported for comparison are from (Abbey, 1980).

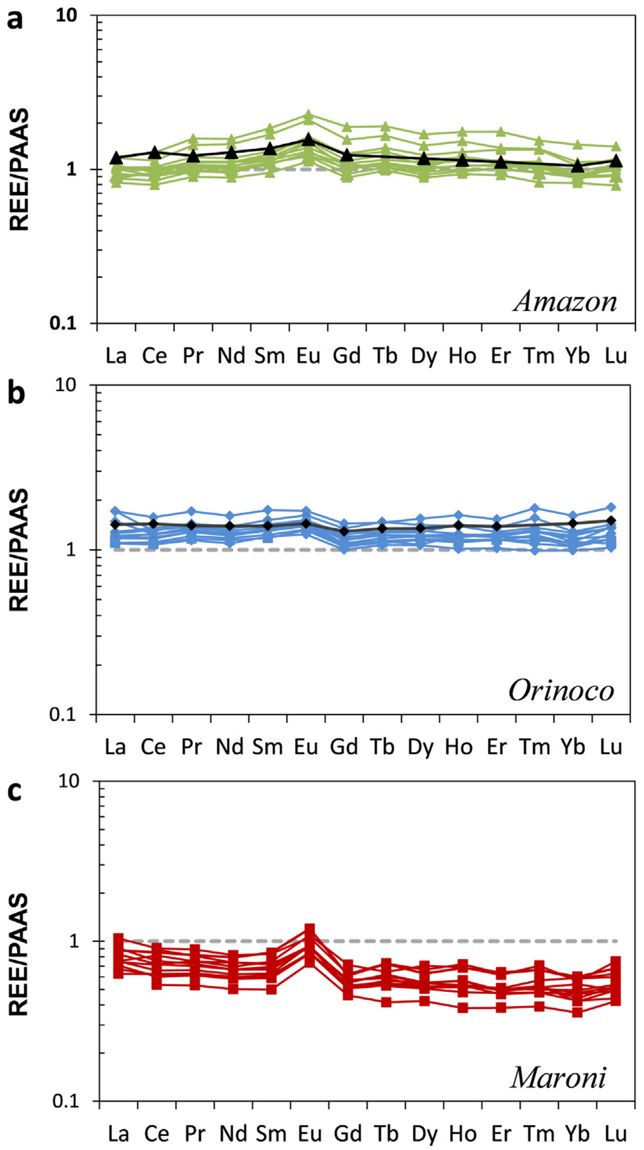

Fig. 6. Rare earth element (REE) concentrations compositions of Amazon, Orinoco and Maroni SPM normalized against PAAS (Pourmand and al., 2012) and corrected with $[Al_2O_3]_{PAAS}/[Al_2O_3]_{Sample}$. REE patterns of clays from Amazon and Orinoco Rivers published by Bayon et al., 2015 are reported for comparison as black curves.

($^{87}Sr/^{86}Sr$ = 0.726–0.73). Measured εNd display a narrow range of εNd values (−14.1 ± 0.3) in full agreement with the range of values previously reported for other Orinoco river-borne sediments (from −13.6 to −14.1; Goldstein et al., 1997; Parra et al., 1997; Bayon et al., 2015). However the Orinoco SPM εNd values are less radiogenic than potential Andean sources (Oriental Cordillera and Subandean zone, Fig. 8), and Andean SPM transported by Apure (−11.7) and Meta (−13.4) Rivers (Goldstein et al., 1997). According to Meade (1994), the Apure and Meta Rivers contribute respectively to 17% and 55% to the total annual solid discharge from the Orinoco River. The εNd signature of SPM transported by the Guaviare River (i.e. a left-bank tributary), which accounts for 23% of the Orinoco SPM discharge, is yet to be determined. Right bank tributaries of the Orinoco are far less radiogenic with respect to εNd (Suapure −19.9; Ventuari-20.5; Caura −21.1; Aro −20.1 to −30.7 and Caroni −25.2; Goldstein et al., 1997; Bayon et al., 2015). These tributaries contribute however for < 5% of the total annual SPM load. Assuming a constant Nd concentration in all SPM, a simple mass balance mixing model would require a Guaviare εNd value to be comprised between −16 and −14.

5.1.3. Amazon River

Compared to PAAS, the Amazon SPM have slightly higher Eu/Eu* and slightly lower Th/Sc ratios, but higher CIA values indicating that the Amazon SPM are slightly less differentiated and more weathered than PAAS. The Sr and Nd isotopic compositions of Amazon SPM measured in this study fall between those reported earlier for the Madeira and Solimões Rivers (Viers et al., 2008) (Fig. 8, 9a). Despite significant dispersion in εNd values for Amazon SPM during the studied hydrological year (between February 2012 and January 2013), the average value (−10.6 ± 0.6) is similar to that observed for the Amazon at Óbidos in June and October 2013 (−10.2 ± 0.1) (Merschel et al., 2017), in the Amazon main channel downstream of Madeira confluence (7 samples; −10.4 ± 0.4; Höppner et al., 2018), in the Amazon delta SPM (−10.7 ± 0.1; Rousseau et al. (2015)), and for the Amazon sub-delta sediments (−10.5 ± 0.1; Bayon et al., 2015). Finally, it is in agreement with a previous estimate (−10.3) calculated based on isotopic composition of Madeira and Solimões SPM collected upstream (Viers et al., 2008). Hence, dispersion of the Amazon SPM εNd values analysed here may reflect variations in the relative sediment contribution from the Madeira (εNd = −11.5, Viers et al., 2008) versus Solimões (εNd = −9.5, Viers et al., 2008) rivers.

5.2. Influence of the hydrological cycle

To discuss the influence of the hydrological cycle on SPM geochemistry we investigate the relationship between monthly variations for elemental and isotopic ratios (Fig. 9) and parameters such as daily river discharge (Qr), SPM concentrations ([SPM]) and fluxes (Qs) according to Eq. (4):

$$Qs = Qr * [SPM] \tag{4}$$

where Qs is the daily SPM flux.

5.2.1. Maroni River

The following characteristics for the Maroni River exhibit intra-annual variations (Fig. 9, Tables 1–3): Al/Si, CIA, Th/Sc, Cr/Th, $^{87}Sr/^{86}Sr$ and εNd. However, none of these ratios display any correlation with hydrological parameters such as [SPM], Qr or Qs (the highest R^2 observed are for Cr/Th vs Qr and CIA vs Qr with respective values of 0.41 and 0.35, all other values being < 0.2). This absence of correlation with the hydrological cycle might be due to the fact that absolute variations in SPM concentrations and discharge over the year are much lower for the Maroni (SPMmax-SPMmin = 29 mg·l^{-1}) than for the Amazon and Orinoco (SPMmax-SPMmin = 152 mg·l^{-1} and 148 mg·l^{-1} respectively) (Fig. 9). Despite this general lack of correlation, some trends can be observed between Qr and geochemical and isotopic ratios, especially during the high water discharge peak, when Cr/Th and εNd reach their minimum and Th/Sc reaches its maximum value. If we compare Cr/Th and Th/Sc ratios for the Maroni SPM with those for the Amazon and Orinoco, the Maroni ratios display a higher variability which likely reflects a source effect (Fig. 10). Except for 2 samples (January and April), a significant correlation is observed between εNd and Cr/Th values of SPM transported by the Maroni River (Fig. 10, R^2 = 0.86), which suggests that sediment mixing between "basic" versus more "acidic" sediment sources controls the geochemical composition of the SPM. While the Maroni River basin is dominated by Paleoproterozoic granitic rocks, it also includes basic rocks forming greenstone belts (Gruau et al., 1985). Hence, the observed co-variations between εNd and Cr/Th most likely reflect changes in the relative contribution of granitic versus basic sediment sourced-regions to the total solid load transported by the river. Evidence that the minimum values of Cr/Th and εNd occur in May, June and July (Fig. 9c) suggests lower contribution of particles derived from the greenstone belts during that period of increasing rainfall and associated river runoff (Anon,

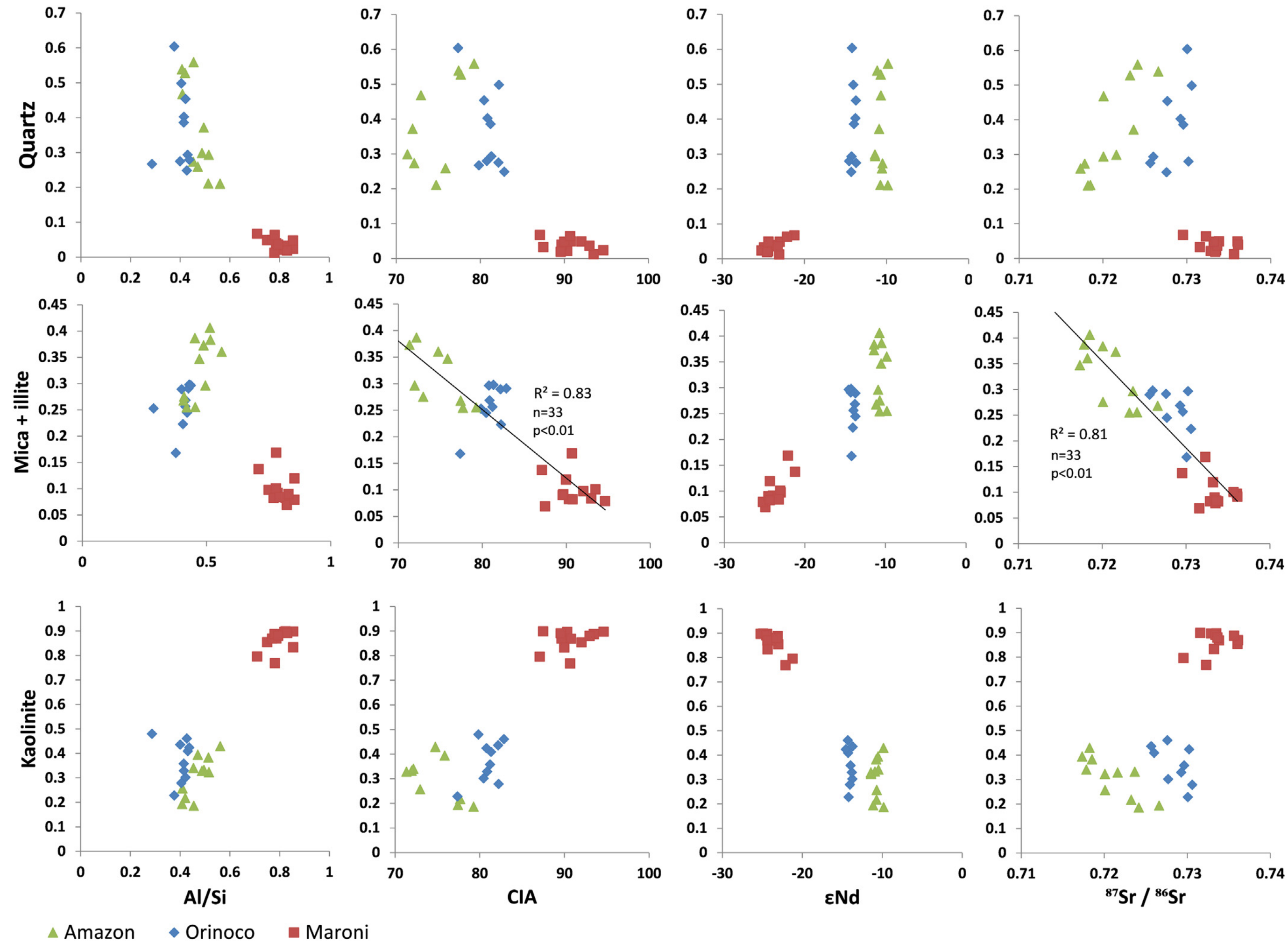

Fig. 7. Cross plot comparing the variation in Al/Si, CIA, εNd and Sr isotopic composition of the analysed SPM as a function of their mineralogy (quartz, mica + illite and kaolinite);

1975) when the Intertropical Convergence Zone (ITCZ) migrates from its southern to northern position (Carvalho and Oyama, 2013; Marengo, 2004).

5.2.2. Orinoco River

Compared to the Maroni, the Orinoco drainage basin covers a much larger area and is characterized by a greater diversity of rock sources and geomorphological settings (i.e. 'young' mountains, sedimentary plain, 'old' cratonic shields). The Orinoco River also displays a particular hydrological regime characterized by relatively high fluctuations of water and sediment discharge and the occurrence of two distinct peaks of SPM concentrations (Fig. 9b).

Despite this particular setting, no correlations of CIA, Th/Sc, Cr/Th, Sr and Nd isotopic compositions with [SPM], Qr or Qs (the highest R^2 observed are for $^{87}Sr/^{86}Sr$ vs Qs and Th/Sc vs Qr with respective values of 0.43 and 0.33 are non-significant for N = 12 and p-value levels of 0.01) is observed (Fig. 9b and Table 1–3). Moreover, compared with the Maroni SPM, the Orinoco SPM displays lower intra-annual variability of geochemical and isotopic ratios. This is particularly notable for Nd and Sr isotopes, suggesting first that Andean sourced sediments are transported all year long to the Ciudad Bolivar station, but also that the geochemical composition of the sediment exported from this area remains relatively homogenous during the hydrological year. The strontium isotopic composition of Orinoco SPM does not fluctuate much over the year, but SPM still display slightly lower $^{87}Sr/^{86}Sr$ ratios are (0.7267 ± 0.0004) between January and April, i.e. during the low water stage, than between May and December (0.7300 ± 0.0004), when water discharge is increasing (Fig. 9). While a similar relationship between discharge and Sr isotopes has also been observed for the Solimões and Madeira Rivers (Viers et al., 2008), the observed SPM geochemical variations in the Orinoco during the year remain quite small, hence suggesting that the Orinoco SPM geochemistry is not controlled by hydrological patterns within the basin.

5.2.3. Amazon River

In the Amazon River basin, Sr isotopic compositions correlate with Qs (R^2 = 0.58; N = 12; p-value < 0.01) and CIA values correlate with [SPM] (R^2 = 0.70; N = 12; p-value < 0.01). Higher CIA values and more radiogenic Sr isotopic composition are observed during low water discharge (i.e. during the dry season), a finding that is somehow similar to that found by Viers et al. (2008) for the SPM of the Solimões and Madeira Rivers, the two main Andean tributaries of the Amazon River.

In contrast with the observations made by Viers et al. (2008) for the Amazon tributaries and by Merschel et al. (2017) for the Amazon at Óbidos, the Nd isotopic compositions display significant seasonal variability, characterized by a gradual εNd increase from −11.4 ± 0.1 in June, during the dry season, to −9.8 ± 0.2 in November to January, during the rainy season (Fig. 9a). This seasonal contrast is in agreement with Höppner et al. (2018) dataset which show a significant difference between SPM sampled near Óbidos in May 2011 (n = 2; −10.9 ± 0.1) and November 2012 (n = 2; −10.2 ± 0.1). At the studied station (Óbidos), suspended particulates are derived from the mixing of

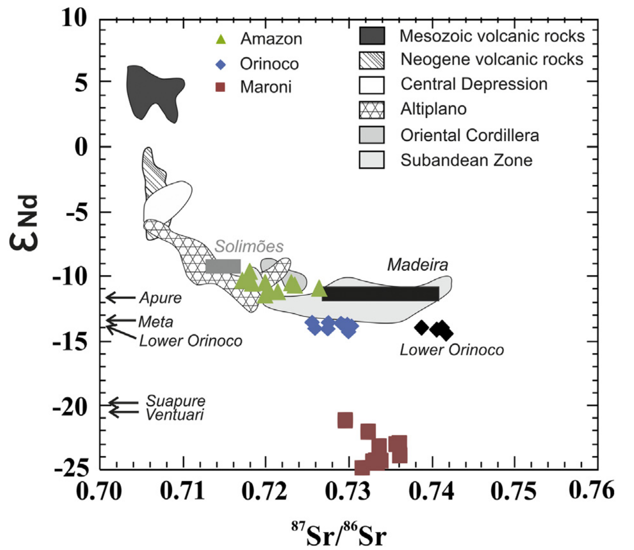

Fig. 8. $^{87}Sr/^{86}Sr$-εNd signatures of Amazon Orinoco and Maroni SPM (this study, green triangles, blue diamonds and red squares) compared with data obtained from various areas of the Andes, the Amazonian and Orinoco basins. Data sources: Quaternary Ecuadorian lavas from (Barragan et al., 1998); Mesozoic and Neogene volcanic rocks from Rogers and Hawkesworth (1989) and from Kay et al. (1994). Data for Cenozoic sedimentary rocks of the Central Depression, Altiplano, Oriental Cordillera and Subandean Zone from Pinto (2003). Madeira and Solimões SPM from Viers et al. (2008). Orinoco and tributaries SPM εNd values from Goldstein et al., 1997 (black arrows). Lower Orinoco sediments and SPM from Parra et al., 1997 (black diamonds). (For interpretation of the references to colour in this figure legend, the reader is referred to the web version of this article.)

particles from the Andes brought by the Solimões and Madeira Rivers (Bouchez et al., 2011; Viers et al., 2008), together with floodplain sediments, whose geochemical compositions also result from variable relative inputs of Solimões and Madeira SPM (Roddaz et al., 2014). The Nd isotopic composition of the Solimões SPM are more radiogenic than those of the Madeira (Viers et al., 2008). As a consequence, we interpret the observed trend towards more radiogenic εNd composition most likely results from increasing sediment contributions from the Solimões River.

Bouchez et al. (2011) demonstrated that the Amazon River is stratified, with Madeira and Solimões SPM being preferentially transported near the surface and Solimões SPM near the channel bottom waters, respectively. Presumably, any increase in discharge and turbulent mixing at Óbidos would enhance mixing of Solimões and Madeira SPM and as a consequence probably would lead to favouring the upwelling of more radiogenic in Nd Solimões SPM. However, it is likely that such mixing would also affect the SPM size distribution and lead to variation in Al/Si ratios. Likewise, Roddaz et al. (2014) estimated that between 52% and 100% of the floodplain deposits proximal to the main channel have low Al/Si ratios (0.15–0.27). If, during the rainy season, increasing bank erosion had favoured the remobilization of such deposits to the Amazon main channel, the observed εNd increase should be accompanied by a decrease of Al/Si ratios. Instead Amazon SPM at Óbidos has higher Al/Si ratios (0.41–0.56) and no correlations between εNd and Al/Si values are observed. Consequently, εNd annual variability in the SPM at Óbidos is unlikely to be controlled by an increase of turbulent mixing condition within the Amazon channel nor by a greater contribution of Amazon floodplain deposits.

To assess the potential control of Madeira versus Solimões Rivers on the observed εNd variability at Óbidos, we consider below the rainfall distribution patterns over the Amazon basin. The south-western part of

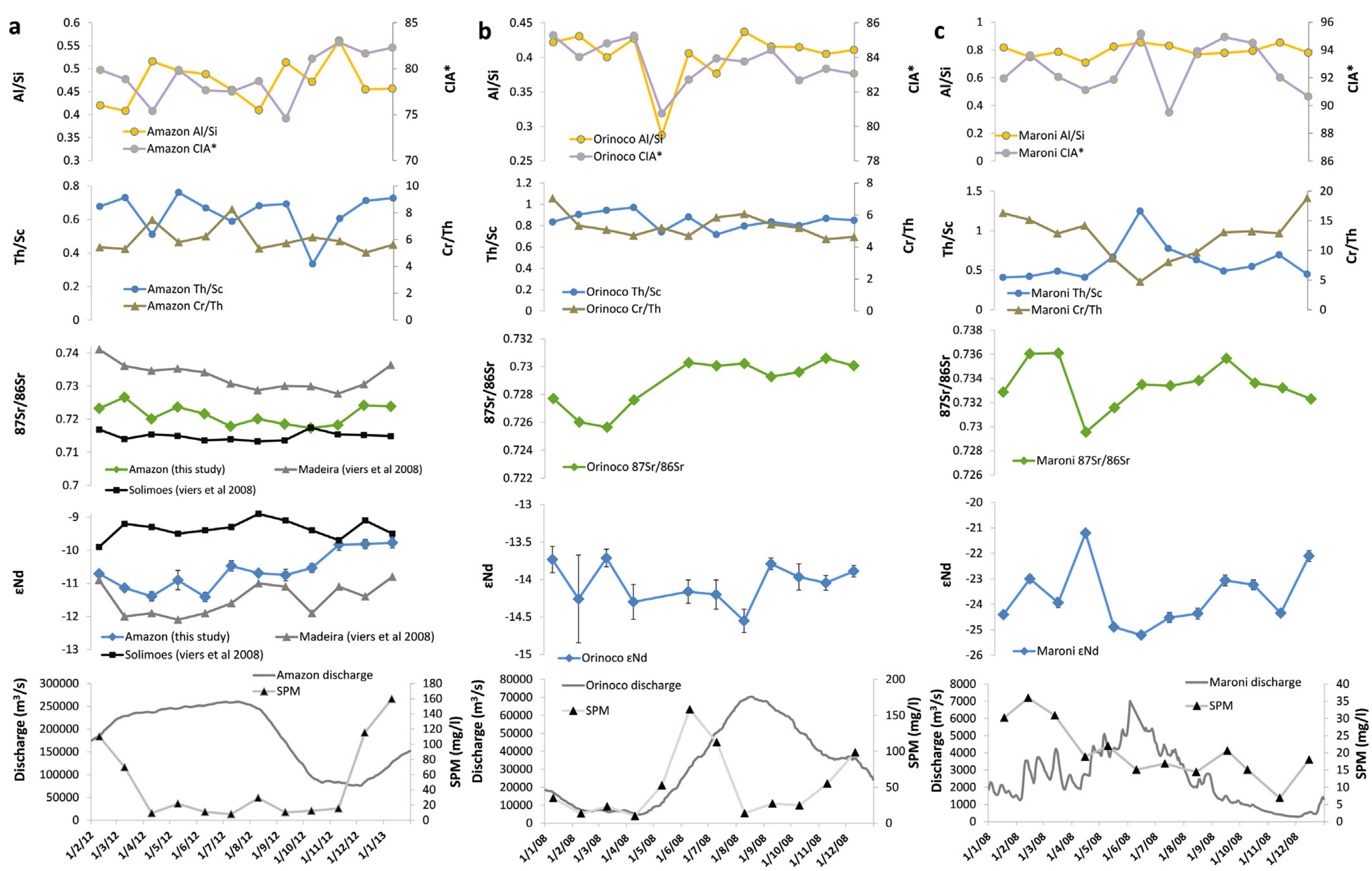

Fig. 9. Plot comparing SPM geochemical data with discharge and SPM concentrations for the Amazon, Orinoco and Maroni Rivers. Viers et al. (2008) $^{87}Sr/^{86}Sr$ and εNd datas from Madeira and Solimões Rivers are reported for comparison.

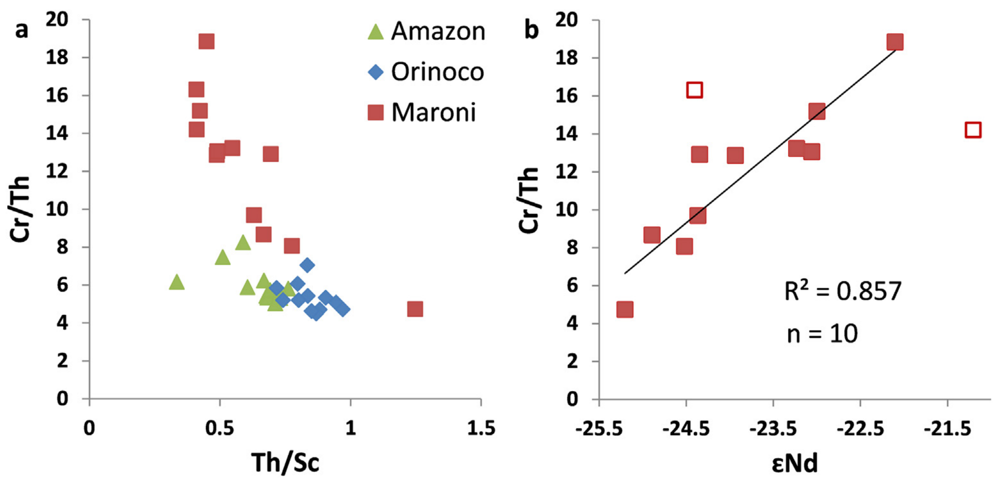

Fig. 10. a) Plot of Cr/Th vs Th/Sc in SPM from the Amazon, Orinoco and Maroni Rivers. b) Plot of Cr/Th vs εNd for Maroni SPM (white-red squares are considered outliers and were not included in regression). (For interpretation of the references to colour in this figure legend, the reader is referred to the web version of this article.)

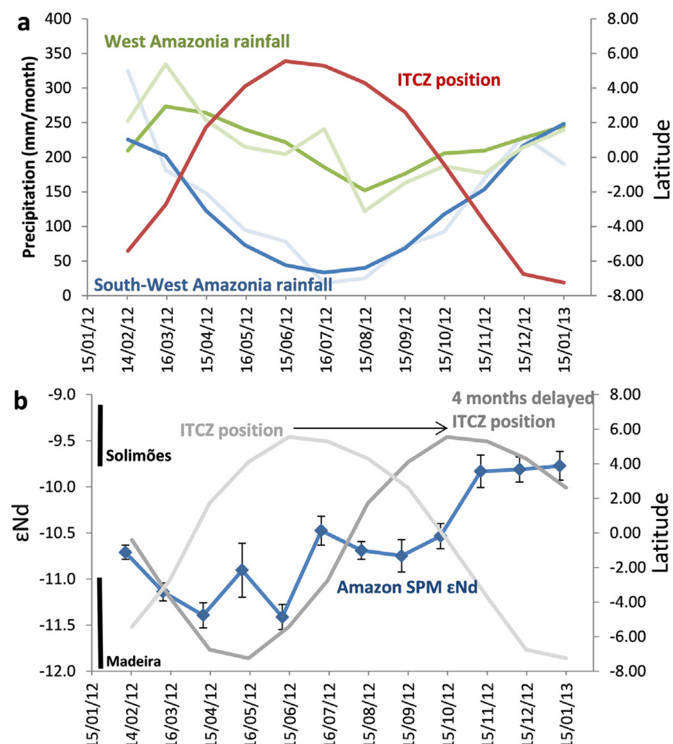

Fig. 11. a) Precipitations over Western Amazonia (6°S-1°N, 79°W-70°W) from 1998 to 2018 (dark green) and in 2012 (light green) and over South-western Amazonia (18°S-12°N, 70°W-62°W) from 1998 to 2018 (dark blue) and in 2012 (light blue) extracted from clim explorer time series (https://climexp.knmi.nl/). Mean position of the ITCZ over South America (75°W-45°W) estimated by Waliser and Gautier (1993). b) Plot of Amazon SPM εNd at Óbidos and the mean position of the ITCZ over South America (75°W-45°W) estimated by Waliser and Gautier (1993). Using a four months lag, the ITCZ position gets in phase with the isotopic signal observed in Óbidos. (For interpretation of the references to colour in this figure legend, the reader is referred to the web version of this article.)

the basin drained by the Madeira River have a marked rainfall seasonality related to South Atlantic Monsoon system (SAMS) activity, it is sensible to the ITCZ migration and mirrors its latitudinal position (Figs. 2, 11). In contrast, the western part of the basin drained by the Solimões River experiences a wet climate during the year with moderate precipitation variations. We suggest that the observed εNd shift between June and November, from Madeira- to Solimões-like compositions, results from seasonal hydroclimate variability across the Amazon Basin. In this case, however, a significant lag in the propagation of the hydrological signal between the Andes and Óbidos needs to be considered as this period corresponds to an increase in rainfall over the upper Madeira region. Such a lag can be difficult to assess over long distances. For example hydrological stations located about 500 km upstream from Óbidos on the Madeira and Solimões Rivers can present a 10–14 days delay in the discharge signal (Mangiarotti et al., 2013). By analogy, and considering the > 2000 km distance that separates Óbidos station to the upstream Andean source regions, a three to four-month delay of the ITCZ latitudinal signal would match well with our εNd SPM signal at Óbidos, hence suggesting that this hypothesis is plausible (Fig. 11). Following this scenario, the observed εNd Amazon SPM from May to June is dominated by Madeira εNd SPM signature, from November to January by Solimões one and from July to October by a mix of Solimões and Madeira.

5.3. Implication for paleoclimate reconstruction

As shown above, suspended matter from the Maroni, the Orinoco and the Amazon (including Solimões and Madeira catchment areas) river basins all display contrasted εNd values and $^{87}Sr/^{86}Sr$ isotopic compositions that can be used to trace the origin of the lithogenic material deposited on adjacent ocean margins. In addition, the Sr and Nd isotopic compositions of analysed SPM may provide interesting constraints on sediment provenance changes related to spatio-temporal variations of rainfall (especially linked to migrations of the tropical rainbelt).

For large rivers such as the Amazon and the Orinoco, the [SPM]-Qr relationship is not straightforward at their outlets due to the hysteresis behaviour caused by a difference in SPM concentrations during the increase and decrease of the river discharge. The amount of sediment exported monthly (Qs) is however mainly controlled by the intensity of precipitation over the Andean part of their hydrographic basin (Armijos et al., 2013a; Armijos et al., 2013b), in addition to other internal sedimentary processes that may take place in the floodplain areas (Dunne et al., 1998; Meade et al., 1985; Santini et al., 2015; Vauchel et al., 2017). Although specific hydrological processes in the floodplains may alter the univocal [SPM]-Qr relationship through dilution effect and various sedimentary effects (Bourgoin et al., 2007; Santini et al., 2015; Vauchel et al., 2017), the geochemistry of exported SPM is mainly controlled by the relative sediment contribution (and consequently rainfall distribution) from the upstream source regions. Hence, if preserved in sedimentary archives, these distinct geochemical signatures may be used to reconstruct past rainfall distribution in the source region.

Erosional patterns and, by inference, rainfall distribution have been reconstructed using Sr–Nd isotopic composition of past sediments,

wherever potential provenance areas display marked geochemical compositions (e.g. Chiessi et al., 2009; Hu et al., 2004). Based on major element compositions of late Quaternary marine sediment, Govin et al. (2014) suggested that the relative proportion of Andean versus lowland sediments increased during periods of high austral summer insolation, in agreement with findings from speleothem records (Cheng et al., 2013; Cruz et al., 2009; Mosblech et al., 2012). Similar changes in sediment provenance between Andes and shield regions were also inferred using Nd—Sr isotopic composition of marine sediments from the Guyana continental slope (Höppner et al., 2018). Our new set of Sr—Nd isotopic data reinforce the view that these proxies can be used in Quaternary sediment archives stored along the tropical South American continental margin for reconstructing the erosional and associated rainfall patterns on continental source regions through time (e.g. Höppner et al., 2018; Zhang et al., 2015). However care must be taken using Sr isotopes for paleoclimate reconstructions as they display a high variability throughout the hydrological cycle. Such variability might be caused by increasing contribution of Sr-rich and Nd-Poor micas during the rainy season that could explain as the observed correlations between mica + illite and Sr isotopic composition (Fig. 7). A similar explanation (i.e. contribution of Sr rich and Nd-poor micas) has been proposed to explain the decoupling between Sr and Nd isotopic composition of marine core sediments from the slope off French Guiana that recorded the last 40 kyr of Amazon River SPM (Höppner et al., 2018) .
.

In this context, the extensive data set presented in our study may provide additional new constraints on sediment provenance that can be used to further discriminate between the various Andean and cratonic sediment source regions (Govin et al., 2014; Höppner et al., 2018) and complement previous paleoclimatic studies conducted on lake sediment records (Baker et al., 2001a; Baker et al., 2001b; Fritz et al., 2007).

6. Conclusions

Our detailed mineralogical and geochemical investigation of SPM transported by the Amazon, Orinoco and Maroni Rivers over a one-year hydrological cycle allowed us to identify distinctive geochemical signatures exported by each of these three basins. These signatures reflect differences in source rock lithology from their corresponding watersheds and their variability are controlled by the annual hydrological cycles. In details:

- The Maroni SPM have higher Al/Si ratios and hence finer grain-size, lower Th/Sc ratios and εNd values (−23.7 ± 1.2) higher Cr/Th, CIA values and Sr isotopic composition when compared with other analysed SPM indicating the Maroni River is exporting less differentiated, older and more weathered detritus than those from other analysed tropical South American rivers SPM. εNd and Cr/Th covariation for Maroni SPM during the hydrological cycle reflect the change in relative contribution of greenstone belt and Paleoproterozoic granitic rocks associated with rainfall distribution heterogeneities linked to ICTZ migration.
- The Orinoco SPM are characterized by distinct CIA values, Th/Sc and Cr/Th and Sr—Nd isotopic compositions (0.7288 ± 0.0018 and εNd = −14.1 ± 0.3, respectively). There is no control of the hydrogical cycle on the geochemistry of Orinoco SPM.
- The Amazon SPM have distinct Th/Sc ratios, CIA values and Sr—Nd isotopic compositions indicating that the Amazon SPM are slightly less differentiated and more weathered than PAAS. The Sr and Nd isotopic compositions of Amazon SPM range between those of the Madeira and Solimões SPM. The Amazon SPM are characterized by significant Sr isotope annual variability (with associated mean and standard deviation of 0.7213 ± 0.0030) correlated with suspended sediments discharge. We also demonstrate a small but significant Nd isotopic variability over the year (with associated mean and standard deviation of −10.6 ± 0.6), from a Madeira- to Solimões-like composition. We relate this variability to seasonal changes in the rainfall distribution patterns across the Amazon basin, associated with latitudinal migrations of the ITCZ.

Consequently, the Nd isotopic composition of past fine-grained sediments deposited on adjacent ocean margins could be used as a proxy for reconstructing past hydroclimate changes over tropical South America, more specifically, to infer the past position of the tropical rain belt and the ITCZ through time.

Acknowledgements

This research was funded by Instituts Carnot ISI-FOR and EDROME. This research was supported by the French Research Institute for Development (IRD), by the HyBAm Observatory (Hydrology and Geochemistry of the Amazon Basin, www.mpl.ird.fr/hybam/) in the framework of its cooperation agreement with the Brazilian Research Centre (CNPq process nos. 492685/2004–05 and 690139/2003–09). We thank the two anonymous reviewers and the editor for their constructive reviews.

References

Aalto, R., Dunne, T., Guyot, J.-L., 2006. Geomorphic controls on Andean denudation rates. J. Geol. 114 (1), 85–99.
Abbey, S., 1980. Studies in “Standard Samples” for use in the general analysis of silicate rocks and minerals. Geostand. Geoanal. Res. 4 (2), 163–190.
Ahlfeld, F., Branisa, L., 1960. Geología de Bolivia. Editorial Don Bosco.
Allègre, C.J., Dupré, B., Négrel, P., Gaillardet, J., 1996. Sr—Nd—Pb isotope systematics in Amazon and Congo river systems: constraints about erosion processes. Chem. Geol. 131 (1–4), 93–112.
Anon, 1975. Climatologie de la Guyane. Contrib. scient. ORSTOM, Tome Secrétariat d'Etat aux D.O.M. - T.O.M., doc mult: 41–59.
Aries, S., Valladon, M., Polvé, M., Dupré, B., 2000. A routine method for oxide and hydroxide interference corrections in ICP-MS chemical analysis of environmental and geological samples. J. Geostand. Geoanal. 24 (1), 19–31.
Armijos, E., Crave, A., Vauchel, P., Fraizy, P., Santini, W., Moquet, J.-S., Arevalo, N., Carranza, J., Guyot, J.-L., 2013a. Suspended sediment dynamics in the Amazon River of Peru. J. S. Am. Earth Sci. 44, 75–84.
Armijos, E., Laraque, A., Barba, S., Bourrel, L., Ceron, C., Lagane, C., Magat, P., Moquet, J.-S., Pombosa, R., Sondag, F., 2013b. Yields of suspended sediment and dissolved solids from the Andean basins of Ecuador. Hydrol. Sci. J. 58 (7), 1478–1494.
Armijos, E., Crave, A., Espinoza, R., Fraizy, P., Dos Santos, A.L.M.R., Sampaio, F., De Oliveira, E., Santini, W., Martinez, J.M., Autin, P., 2017. Measuring and modeling vertical gradients in suspended sediments in the Solimões/Amazon River. Hydrol. Process. 31 (3), 654–667.
Baker, P.A., Rigsby, C.A., Seltzer, G.O., Fritz, S.C., Lowenstein, T.K., Bacher, N.P., Veliz, C., 2001a. Tropical climate changes at millennial and orbital timescales on the Bolivian Altiplano. Nature 409 (6821), 698.
Baker, P.A., Seltzer, G.O., Fritz, S.C., Dunbar, R.B., Grove, M.J., Tapia, P.M., Cross, S.L., Rowe, H.D., Broda, J.P., 2001b. The history of South American tropical precipitation for the past 25,000 years. Science 291 (5504), 640–643.
Baldock, J.W., 1982. Geología del Ecuador, Boletín de Explicación del Mapa Geológico dela Republica del Ecuador al 1:1 000 000. (Quito Ecuador).
Barragan, R., Geist, D., Hall, M., Larson, P., Kurz, M., 1998. Subduction controls on the compositions of lavas from the Ecuadorian Andes. Earth Planet. Sci. Lett. 154, 153–166.
Basu, A.R., Sharma, M., DeCelles, P.G., 1990. Nd, Sr-isotopic provenance and trace element geochemistry of Amazonian foreland basin fluvial sands, Bolivia and Peru: implications for ensialic Andean orogeny. Earth Planet. Sci. Lett. 100 (1–3), 1–17.
Bayon, G., Toucanne, S., Skonieczny, C., André, L., Bermell, S., Cheron, S., Dennielou, B., Etoubleau, J., Freslon, N., Gauchery, T., Germain, Y., Jorry, S.J., Ménot, G., Monin, L., Ponzevera, E., Rouget, M.L., Tachikawa, K., Barrat, J.A., 2015. Rare earth elements and neodymium isotopes in world river sediments revisited. Geochim. Cosmochim. Acta 170, 17–38.
Bayon, G., Skonieczny, C., Delvigne, C., Toucanne, S., Bermell, S., Ponzevera, E., Andre, L., 2016. Environmental Hf–Nd isotopic decoupling in World river clays. Earth Planet. Sci. Lett. 438, 25–36.
Bonnet, M.P., Barroux, G., Martinez, J.M., Seyler, F., Moreira-Turcq, P., Cochonneau, G., Melack, J.M., Boaventura, G., Maurice-Bourgoin, L., Leon, J.G., Roux, E., Calmant, S., Kosuth, P., Guyot, J.L., Seyler, P., 2008. Floodplain hydrology in an Amazon floodplain lake (Lago Grande de Curuai). J. Hydrol. 349 (1–2), 18–30.
Bouchez, J., Gaillardet, J., France-Lanord, C., Maurice, L., Dutra-Maia, P., 2011. Grain size control of river suspended sediment geochemistry: clues from Amazon River depth profiles. Geochem. Geophys. Geosyst. 12 (3), Q03008.
Bouchez, J., Moquet, J.-S., Espinoza, J.C., Martinez, J.-M., Guyot, J.-L., Lagane, C., Filizola, N., Noriega, L., Hidalgo Sanchez, L., Pombosa, R., 2017. River mixing in the Amazon as a driver of concentration-discharge relationships. Water Resour. Res. 53 (11), 8660–8685.

Bourgoin, L.M., et al., 2007. Temporal dynamics of water and sediment exchanges between the Curuaí floodplain and the Amazon River, Brazil. J. Hydrol. 335 (1), 140–156.
Callède, J., Cochonneau, J., Ronchail, F., Vieira Alvez, J., Guyot, J.-L., Guimarães, V.S., Olivera, E. de, 2010. Les apports en eau de l'Amazone à l'Océan Atlantique. Rev. Sci. Eau 23 (3), 247–273.
Carvalho, M.Â.V.d., Oyama, M.D., 2013. Variabilidade da largura e intensidade da Zona de Convergência Intertropical atlântica: aspectos observacionais. Revista Brasileira de meteorología 28, 305–316.
Cheng, H., Sinha, A., Cruz, Francisco W., Wang, X., Edwards, R.L., d'Horta, F.M., Ribas, C.C., Vuille, M., Stott, L.D., Auler, A.S., 2013. Climate change patterns in Amazonia and biodiversity. Nat. Commun. 4, 1411.
Chiessi, C.M., Mulitza, S., Pätzold, J., Wefer, G., Marengo, J.A., 2009. Possible impact of the Atlantic Multidecadal oscillation on the South American summer monsoon. Geophys. Res. Lett. 36 (21).
Cruz, F.W., Vuille, M., Burns, Stephen J., Wang, X., Cheng, H., Werner, M., Edwards, R.L., Karmann, I., Auler, A.S., Nguyen, H., 2009. Orbitally driven east–west antiphasing of South American precipitation. Nat. Geosci. 2 (3), 210.
Cullers, R.L., 2000. The geochemistry of shales, siltstones and sandstones of Pennsylvanian–Permian age, Colorado, USA: implications for provenance and metamorphic studies. Lithos 51 (3), 181–203.
Dai, A., Trenberth, K.E., 2002. Estimates of freshwater discharge from continents: Latitudinal and seasonal variations. J. Hydrometeorol. 3 (6), 660–687.
Dosseto, A., Bourdon, B., Gaillardet, J., Allègre, C.J., Filizola, N., 2006. Time scale and conditions of weathering under tropical climate: Study of the Amazon basin with U-series. Geochim. Cosmochim. Acta 70 (1), 71–89.
Dunne, T., Mertes, L.A., Meade, R.H., Richey, J.E., Forsberg, B.R., 1998. Exchanges of sediment between the flood plain and channel of the Amazon River in Brazil. Geol. Soc. Am. Bull. 110 (4), 450–467.
Edmond, J., Palmer, M., Measures, C., Grant, B., Stallard, R., 1995. The fluvial geochemistry and denudation rate of the Guayana Shield in Venezuela, Colombia, and Brazil. Geochim. Cosmochim. Acta 59 (16), 3301–3325.
Edmond, J., Palmer, M., Brown, E., Huh, Y., 1996. Fluvial geochemistry of the eastern slope of the northeastern Andes and its foredeep in the drainage of the Orinoco in Colombia and Venezuela. Geochim. Cosmochim. Acta 60 (16), 2949–2974.
Espinoza Villar, J.C., Ronchail, J., Guyot, J.-L., Cochonneau, G., Naziano, F., Lavado, W., De Oliveira, E., Pombosa, R., Vauchel, P., 2009. Spatio-temporal rainfall variability in the Amazon basin countries (Brazil, Peru, Bolivia, Colombia, and Ecuador). Int. J. Climatol. 29 (11), 1574–1594.
Filizola, N., Guyot, J.L., 2009. Suspended sediment yields in the Amazon basin: an assessment using the Brazilian national data set. Hydrol. Process. 23 (22), 3207–3215.
Filizola, N., Guyot, J.-L., 2004. The use of Doppler technology for suspended sediment discharge determination in the Amazon river. Hydrol. Sci. J. Environ. Monit. 49 (1), 143–153.
Filizola, N., Guyot, J.-L., Wittmann, H., Martinez, J.-M., de Oliveira, E., 2011. The significance of suspended sediment transport determination on the Amazonian hydrological scenario. In: Sediment transport in aquatic environments. InTech.
Fritz, S.C., Baker, P.A., Seltzer, G.O., Ballantyne, A., Tapia, P., Cheng, H., Edwards, R.L., 2007. Quaternary glaciation and hydrologic variation in the South American tropics as reconstructed from the Lake Titicaca drilling project. Quat. Res. 68 (3), 410–420.
Furch, K., Junk, W., 1982. Seasonal nutrient dynamics in aAmazonian floodplain lake. Arch. Hydrobiol. 128 (3), 227–285.
Gaillardet, J., Dupre, B., Allègre, C.J., Négrel, P., 1997. Chemical and physical denudation in the Amazon River Basin. Chem. Geol. 142 (3–4), 141–173.
Gaillardet, J., Dupre, B., Allegre, C.J., 1999. Geochemistry of large river suspended sediments: Silicate weathering or recycling tracer? Geochim. Cosmochim. Acta 63 (23–24), 4037–4051.
Galy, V., France-Lanord, C., Beyssac, O., Faure, P., Kudrass, H., Palhol, F., 2007. Efficient organic carbon burial in the Bengal fan sustained by the Himalayan erosional system. Nature 450 (7168), 407–U6.
Gibbs, R.J., 1967. The geochemistry of the Amazon river system: part I. the factors that control the salinity and the composition and concentration of the suspended solids. Geol. Soc. Am. Bull. 78 (10), 1203–1232.
Goldstein, S., Arndt, N., Stallard, R., 1997. The history of a continent from U-Pb ages of zircons from Orinoco River sand and Sm-Nd isotopes in Orinoco basin river sediments. Chem. Geol. 139 (1–4), 271–286.
Goldstein, S.J., Jacobsen, S.B., 1988. Nd and Sr isotopic systematics of river water suspended material: implications for crustal evolution. Earth Planet. Sci. Lett. 87 (3), 249–265.
Goldstein, S.L., O'Nions, R.K., Hamilton, P.J., 1984. A Sm-Nd isotopic study of atmospheric dusts and particulates from major river systems. Earth Planet. Sci. Lett. 70 (2), 221–236.
Govin, A., Chiessi, C.M., Zabel, M., Sawakuchi, A.O., Heslop, D., Hörner, T., Zhang, Y., Mulitza, S., 2014. Terrigenous input off northern South America driven by changes in Amazonian climate and the North Brazil current retroflection during the last 250 ka. Clim. Past 10 (2), 843–862.
Gruau, G., Martin, H., Leveque, B., Capdevila, R., Marot, A., 1985. Rb—Sr and Sm—Nd geochronology of lower Proterozoic granite—greenstone terrains in French Guiana, South America. Precambrian Res. 30 (1), 63–80.
Guimberteau, M., Drapeau, G., Ronchail, J., Sultan, B., Polcher, J., Martinez, J.-M., Prigent, C., Guyot, J.-L., Cochonneau, G., Espinoza Villar, J.C., 2012. Discharge simulation in the sub-basins of the Amazon using ORCHIDEE forced by new datasets. Hydrol. Earth Syst. Sci. 16 (3), 11171–11232.
Guyot, J.L., Jouanneau, J.M., Wasson, J.G., 1999. Characterisation of river bed and suspended sediments in the Rio Madeira drainage basin (Bolivian Amazonia). J. S. Am. Earth Sci. 12 (4), 401–410.
Guyot, J.L., Filizola, N., Laraque, A., 2005. The suspended sediment flux of the River Aazon at Obidos, Brazil, 1995-2003. In: Walling, D.E., Horowitz, A.J. (Eds.), Sediment Budgets 1. Iahs Publication, pp. 347–354.
Guyot, J.L., Jouanneau, J.M., Soares, L., Boaventura, G.R., Maillet, N., Lagane, C., 2007. Clay mineral composition of river sediments in the Amazon Basin. Catena 71 (2), 340–356.
Hamilton, S.K., 2010. Biogeochemical implications of climate change for tropical rivers and floodplains. Hydrobiologia 657 (1), 19–35.
Hodell, D.A., Kamenov, G.D., Hathorne, E.C., Zachos, J.C., Röhl, U., Westerhold, T., 2007. Variations in the strontium isotope composition of seawater during the Paleocene and early Eocene from ODP Leg 208 (Walvis Ridge). Geochem. Geophys. Geosyst. 8 (9).
Hoorn, C., Bogotá-A, G.R., Romero-Baez, M., Lammertsma, E.I., Flantua, S.G.A., Dantas, E.L., Dino, R., do Carmo, D.A., Chemale, F., 2017. The Amazon at sea: Onset and stages of the Amazon river from a marine record, with special reference to Neogene plant turnover in the drainage basin. Glob. Planet. Chang., 153: 51–65.
Höppner, N., Lucassen, F., Chiessi, C.M., Sawakuchi, A.O., Kasemann, S.A., 2018. Holocene provenance shift of suspended particulate matter in the Amazon river basin. Quat. Sci. Rev. 190, 66–80.
Hu, C., Montgomery, E.T., Schmitt, R.W., Muller-Karger, F.E., 2004. The dispersal of the Amazon and Orinoco river water in the tropical Atlantic and Caribbean sea: observation from space and S-PALACE floats. Deep-Sea Res. II Top. Stud. Oceanogr. 51 (10 − 11), 1151–1171.
INGEMMET, 1999. Geological Maps, Scale 1:100, 000. In: INGEMMET-Instituto Geologico y Metalurgico del Peru, Lima, Peru.
Jacobsen, S.B., Wasserburg, G.J., 1980. Sm-Nd isotopic evolution of chondrites. Earth Planet. Sci. Lett. 50 (1), 139–155.
Junk, W., Sioli, H., 1984. The Amazon: Limnology and Landscape Ecology of a Mighty Tropical River and its Basin 264.
Kay, S., Coira, B., Viramonte, J., 1994. Young mafic back arc volcanic rocks as indicators of continental lithospheric delamination beneath the Argentina Puna plateau, central Andes. J. Geophys. Res. 99, 24323–24339.
Konhauser, K.O., Fyfe, W.S., Kronberg, B.I., 1994. Multi-element chemistry of some Amazonian waters and soils. Chem. Geol. 111 (1–4), 155–175.
Laraque, A., Castellanos, B., Steiger, J., Lòpez, J.L., Pandi, A., Rodriguez, M., Rosales, J., Adèle, G., Perez, J., Lagane, C., 2013a. A comparison of the suspended and dissolved matter dynamics of two large inter-tropical rivers draining into the Atlantic Ocean: the Congo and the Orinoco. Hydrol. Process. 27 (15), 2153–2170.
Laraque, A., Moquet, J.-S., Alkattan, R., Steiger, J., Mora, A., Adèle, G., Castellanos, B., Lagane, C., Lopez, José L., Perez, J., Rodriguez, M., Rosales, J., 2013b. Seasonal variability of total dissolved fluxes and origin of major dissolved elements within a large tropical river: the Orinoco, Venezuela. J. S. Am. Earth Sci. 44, 4–17.
Lugmair, G.W., Shimamura, T., Lewis, R.S., Anders, E., 1983. Samarium-146 in the early solar system: evidence from Neodymium in the Allende meteorite. Science 222 (4627), 1015–1018.
Mangiarotti, S., Martinez, J.-M., Bonnet, M.-P., Buarque, D.C., Filizola, N., Mazzega, P., 2013. Discharge and suspended sediment flux estimated along the mainstream of the Amazon and the Madeira Rivers (from in situ and MODIS Satellite Data). Int. J. Appl. Earth Obs. Geoinf. 21, 341–355.
Marengo, J., 2004. Interdecadal variability and trends of rainfall across the Amazon basin. Theor. Appl. Climatol. 78 (1), 79–96.
Marengo, J., Liebmann, B., Grimm, A.M., Misra, V., Silva Dias, P.L., Cavalcanti, I.F.A., Carvalho, L.M.V., Berbery, E.H., Ambrizzi, T., Vera, C.S., 2012. Recent developments on the South American monsoon system. Int. J. Climatol. 32 (1), 1–21.
Martinelli, L.A., Victoria, R.L., Dematte, J.L.I., Richey, J.E., Devol, A.H., 1993. Chemical and mineralogical composition of Amazon river floodplain sediments, Brazil. Appl. Geochem. 8 (4), 391–402.
Martinez, J.M., Le Toan, T., 2007. Mapping of flood dynamics and spatial distribution of vegetation in the Amazon floodplain using multitemporal SAR data. Remote Sens. Environ. 108, 209–223.
Martinez, J.M., Guyot, J.L., Filizola, N., Sondag, F., 2009. Increase in suspended sediment discharge of the Amazon River assessed by monitoring network and satellite data. Catena 79 (3), 257–264.
McLennan, S., Hemming, S., McDaniel, D., Hanson, G., 1993. Geochemical approaches to sedimentation, provenance, and tectonics. Geol. Soc. Am. Spec. Pap. 284, 21–40.
Meade, R.H., 1994. Suspended sediments of the modern Amazon and Orinoco rivers. Quat. Int., 21(0): 29–39.
Meade, R.H., Dunne, T., Richey, J.E., Santos, U.D.M., Salati, E., 1985. Storage and remobilization of suspended sediment in the lower amazon river of Brazil. Science 228, 488–490.
Merschel, G., Bau, M., Schmidt, K., Münker, C., Dantas, E.L., 2017. Hafnium and neodymium isotopes and REY distribution in the truly dissolved, nanoparticulate/colloidal and suspended loads of rivers in the Amazon Basin, Brazil. Geochim. Cosmochim. Acta 213, 383–399.
Mertes, L.A., Dunne, T., Martinelli, L.A., 1996. Channel-floodplain geomorphology along the Solimões-Amazon river, Brazil. Geol. Soc. Am. Bull. 108 (9), 1089–1107.
Meybeck, M., 1993. Riverine transport of atmospheric carbon - sources, global typology and budget. Water Air Soil Pollut. 70 (1–4), 443–463.
Milliman, J., Farnsworth, K., 2011a. Runoff, Erosion, and Delivery to the Coastal Ocean. River Discharge to the Coastal Ocean: A Global Synthesis. Cambridge University Press, Cambridge, UK, pp. 13–69.
Milliman, J.D., Farnsworth, K.L., 2011b. River Discharge to the Coastal Ocean. A Global Synthesis. Cambridge University Press.
Milliman, J.D., Meade, R.H., 1983. World-wide dlivery of river sediment to the oceans. J. Geol. 91, 1–21.
Molina-Carpio, J., Espinoza, J.C., Vauchel, P., Ronchail, J., Gutierrez Caloir, B., Guyot, J.-L., Noriega, Luis, et al., 2017. Hydroclimatology of the Upper Madeira river basin:

spatio-temporal variability and trends. Hydrol. Sci. J. 62 (6), 911–927.
Moquet, J.-S., Guyot, J.-L., Crave, A., Viers, J., Filizola, N., Martinez, J.-M., Oliveira, T.C., Sánchez, L.S.H., Lagane, C., Casimiro, W.S.L., 2016. Amazon River dissolved load: temporal dynamics and annual budget from the Andes to the ocean. Environ. Sci. Pollut. Res. 23 (12), 11405–11429.
Mora, A., Laraque, A., Moreira-Turcq, P., Alfonso, J.A., 2014. Temporal variation and fluxes of dissolved and particulate organic carbon in the Apure, Caura and Orinoco rivers, Venezuela. J. S. Am. Earth Sci. 54, 47–56.
Mosblech, N.A., Bush, M.B., Gosling, W.D., Hodell, D., Thomas, L., Van Calsteren, P., Correa-Metrio, A., Valencia, B.G., Curtis, J., Van Woesik, R., 2012. North Atlantic forcing of Amazonian precipitation during the last ice age. Nat. Geosci. 5 (11), 817.
Négrel, P., Lachassagne, P., 2000. Geochemistry of the Maroni River (French Guiana) during the low water stage: implications for water–rock interaction and groundwater characteristics. J. Hydrol. 237 (3), 212–233.
Nesbitt, H., Young, G., 1982. Early Proterozoic climates and plate motions inferred from major element chemistry of lutites. Nature 299 (5885), 715–717.
Parra, M., Faugères, J.-C., Grousset, F., Pujol, C., 1997. Sr-Nd isotopes as tracers of fine-grained detrital sediments: the South-Barbados accretionary prism during the last 150 kyr. Mar. Geol. 136 (3–4), 225–243.
Pinet, S., Martinez, J.-M., Ouillon, S., Lartiges, B., Villar, R.E., 2017. Variability of apparent and inherent optical properties of sediment-laden waters in large river basins–lessons from in situ measurements and bio-optical modeling. Opt. Express 25 (8), A283–A310.
Pinto, L., 2003. Traçage de l'érosion Cénozoïque des Andes Centrales à l'aide dela minéralogie et de la géochmie des sédiements (Nord du Chili et Nord-Ouest de la Bolivie). PhD Thesis. University Paul Sabatier, Toulouse (196 pp).
Pourmand, A., Dauphas, N., Ireland, T.J., 2012. A novel extraction chromatography and MC-ICP-MS technique for rapid analysis of REE, Sc and Y: revising CI-chondrite and Post-Archean Australian Shale (PAAS) abundances. Chem. Geol. 291, 38–54.
Raia, A., Cavalcanti, I.F.A., 2008. The life cycle of the South American monsoon system. J. Clim. 21 (23), 6227–6246.
Roddaz, M., Viers, J., Brusset, S., Baby, P., Hérail, G., 2005. Sediment provenances and drainage evolution of the Neogene Amazonian foreland basin. Earth Planet. Sci. Lett. 239 (1–2), 57–78.
Roddaz, M., Viers, J., Brusset, S., Baby, P., Boucayrand, C., Hérail, G., 2006. Controls on weathering and provenance in the Amazonian foreland basin: Insights from major and trace element geochemistry of Neogene Amazonian sediments. Chem. Geol. 226 (1–2), 31–65.
Roddaz, M., Viers, J., Moreira-Turcq, P., Blondel, C., Sondag, F., Guyot, J.-L., Moreira, L., 2014. Evidence for the control of the geochemistry of Amazonian floodplain sediments by stratification of suspended sediments in the Amazon. Chem. Geol. 387, 101–110.
Rogers, G., Hawkesworth, C.J., 1989. A geochemical traverse across the North Chilean Andes: evidence for crust generation from the mantle wedge. Earth Planet. Sci. Lett. 91, 271–275.
Rousseau, T.C.C., Sonke, J.E., Chmeleff, J., van Beek, P., Souhaut, M., Boaventura, G., Seyler, P., Jeandel, C., 2015. Rapid neodymium release to marine waters from lithogenic sediments in the Amazon estuary. Nat. Commun. 6, 7592.
Santini, W., Martinez, J.-M., Espinoza-Villar, R., Cochonneau, G., Vauchel, P., Moquet, J.-S., Baby, P., Espinoza, J.-C., Lavado, W., Carranza, J., 2015. Sediment budget in the Ucayali River basin, an Andean tributary of the Amazon River. In: Proceedings of the International Association of Hydrological Sciences. 367. pp. 320.
Sawakuchi, Jain, M., Mineli, T.D., Nogueira, L., Bertassoli, D.J., Häggi, C., Sawakuchi, H.O., Pupim, F.N., Grohmann, C.H., Chiessi, C.M., 2018. Luminescence of quartz and feldspar fingerprints provenance and correlates with the source area denudation in the Amazon River basin. Earth Planet. Sci. Lett. 492, 152–162.
SERGEOMIN and YPFB, 2000. Mapa geológico de Bolivia, Esc. 1:1.000.000. S.N.d.G.y. Minería-(SERGEOMIN) and Y.P.F.B. (YPFB) (Editors), La Paz.
van Soelen, E.E., et al., 2017. A 30 Ma history of the Amazon river inferred from terrigenous sediments and organic matter on the Ceará rise. Earth Planet. Sci. Lett. 474, 40–48.
Sondag, F., Guyot, J.-L., Moquet, J.-S., Laraque, A., Adele, G., Cochonneau, G., Doudou, J.-C., Lagane, C., Vauchel, P., 2010. Suspended sediment and dissolved load budgets of two Amazonian rivers from the Guiana Shield: Maroni River at Langa Tabiki and Oyapock River at Saut Maripa (French Guiana). Hydrol. Process. 24 (11), 1433–1445.
Syvitski, J.P., Milliman, J.D., 2007. Geology, geography, and humans battle for dominance over the delivery of fluvial sediment to the coastal ocean. J. Geol. 115 (1), 1–19.
Syvitski, J.P., Peckham, S.D., Hilberman, R., Mulder, T., 2003. Predicting the terrestrial flux of sediment to the global ocean: a planetary perspective. Sediment. Geol. 162 (1), 5–24.
Syvitski, J.P., Cohen, S., Kettner, A.J., Brakenridge, G.R., 2014. How important and different are tropical rivers?—an overview. Geomorphology 227, 5–17.
Vauchel, P., Santini, W., Guyot, J.-L., Moquet, J.-S., Martinez, J.-M., Espinoza, J.C., Baby, P., Fuertes, O., Noriega, L., Puita, O., 2017. A reassessment of the suspended sediment load in the Madeira River basin from the Andes of Peru and Bolivia to the Amazon River in Brazil, based on 10 years of data from the HYBAM monitoring programme. J. Hydrol. 553, 35–48.
Viers, J., Barroux, G., Pinelli, M., Seyler, P., Oliva, P., Dupré, B., Boaventura, G.R., 2005. The influence of the Amazonian floodplain ecosystems on the trace element dynamics of the Amazon River mainstem (Brazil). Sci. Total Environ. 339 (1–3), 219–232.
Viers, J., Roddaz, M., Filizola, N., Guyot, J.-L., Sondag, F., Brunet, P., Zouiten, C., Boucayrand, C., Martin, F., Boaventura, G.R., 2008. Seasonal and provenance controls on Nd-Sr isotopic compositions of Amazon rivers suspended sediments and implications for Nd and Sr fluxes exported to the Atlantic Ocean. Earth Planet. Sci. Lett. 274 (3–4), 511–523.
Vital, H., Stattegger, K., 2000. Major and trace elements of stream sediments from the lowermost Amazon River. Chem. Geol. 168 (1–2), 151–168.
Waliser, D.E., Gautier, C., 1993. A satellite-derived climatology of the ITCZ. J. Clim. 6 (11), 2162–2174.
Wittmann, H., Von Blanckenburg, F., Maurice, L., Guyot, J.-L., Kubik, P., 2011. Recycling of Amazon floodplain sediment quantified by cosmogenic 26Al and 10Be. Geology 39 (5), 467–470.
Zhang, Y., Chiessi, C.M., Mulitza, S., Zabel, M., Trindade, R.I.F., Hollanda, M.H.B.M., Dantas, E.L., Govin, A., Tiedemann, R., Wefer, G., 2015. Origin of increased terrigenous supply to the NE South American continental margin during Heinrich Stadial 1 and the Younger Dryas. Earth Planet. Sci. Lett. 432, 493–500.
Zhou, J., Lau, K., 1998. Does a monsoon climate exist over South America? J. Clim. 11 (5), 1020–1040.